Annual Report on

Evaluating the Effects of Moisture on the Thermal Protective Performance of Firefighter Protective Clothing in Low Level Heat Exposures

Submitted to

National Institute of Standards and Technology

from

The Center for Research on Textile Protection and Comfort (T-PACC)
NC State University
Raleigh, NC 27695-8301

NIST Award No. 60 NAN B9 D0092

Annual Report on

Evaluating the Effects of Moisture on the Thermal Protective Performance of Firefighter Protective Clothing in Low Level Heat Exposures

Submitted to

National Institute of Standards and Technology

from

The Center for Research on Textile Protection and Comfort (T-PACC)
NC State University
Raleigh, NC 27695-8301

NIST Award No. 60 NAN B9 D0092

Introduction

The Center for Research on Textile Protection and Comfort (T-PACC) at North Carolina State University is conducting a project which has, as its primary objective, developing an understanding of how the levels and distribution of moisture in firefighter turnout systems and resultant conditions may exacerbate the potential for bum injury in low level heat exposures. The purpose of this report is to summarize progress made, to date, in this ongoing project and to discuss the objectives for the second year of the program.

Summary of Progress

The accomplishments made to date can be summarized as follows:

- Sophisticated laboratory moisture delivery systems have been used to study ways in which moisture is absorbed and distributed in firefighter turnout composites. These studies have provided the foundation for the following outcome:

  - A practical laboratory preconditioning protocol has been developed for use in testing moisture effects on the thermal protective performance of firefighter composites in low level heat exposures. This preconditioning protocol has been shown to reproducibly introduce moisture at levels and distributions that reasonably simulate moisture absorption in firefighter turnout systems exposed to perspiration from a sweating firefighter.

Progress has been made toward the development and evaluation of thermal sensors suitable for use in evaluating thermal protection in low level heat exposures:

- Laboratory experiments have been conducted to evaluate and compare the response of several different thermal sensors, including NCSU's Pyrocal and water cooled sensors to low level heat exposure. The RPP test platform is being used to evaluate response to exposures ranging from 2.5 to 10 kw/m^2. Comparative evaluation of the merits of skin model sensor technologies for low level heat tests is ongoing.

- An experimental series has been conducted to show moisture effects on thermal protective performance in various low level heat exposures.

The second year of this project will be devoted to validation of moisture preconditioning protocols and thermal sensors, and to a full analysis of moisture effects on bum potential.

Moisture Preconditioning Protocols

A major obstacle in the development test methodology for this application is the availability of moisture preconditioning protocols for turnout materials. There is also a lack of basic understanding of how moisture is absorbed in turnout systems when exposed, either to perspiration from a sweating firefighter, or to water from a fire ground source.

Sweat Absorption in Firefighter Turnouts

The optimum moisture preconditioning protocol should simulate both the amount and distribution of moisture absorbed by turnout clothing worn by firefighters. Figure 1 shows how moisture accumulates in different components of firefighters' clothing system in wear. These data, extracted from recently completed physiological studies on the effects of turnout breathability on firefighter heat stress and comfort (1-3), show that the highest percentage of moisture accumulates in absorbent clothing or layers in closest contact with sweat-wetted skin. An absorbent t-shirt material absorbs moisture levels that approach saturation (> 90%). In comparison, turnout garments, worn over a t-shirt and station uniform, absorb moisture in amounts that are significantly below saturation levels (1.5 - 15%). Within individual fabric layers of the turnout composite, moisture is absorbed primarily by the thermal liner component (Figure 2). Moisture absorption, and distribution within the turnout, are determined by the moisture absorption capacity of the thermal liner, by the breathability of the moisture barrier, and by the sweat output in wear. More moisture is absorbed by turnout liners that incorporate thicker thermal liners, principally because thicker thermal liners have greater capacity to contain moisture than thinner liner components.

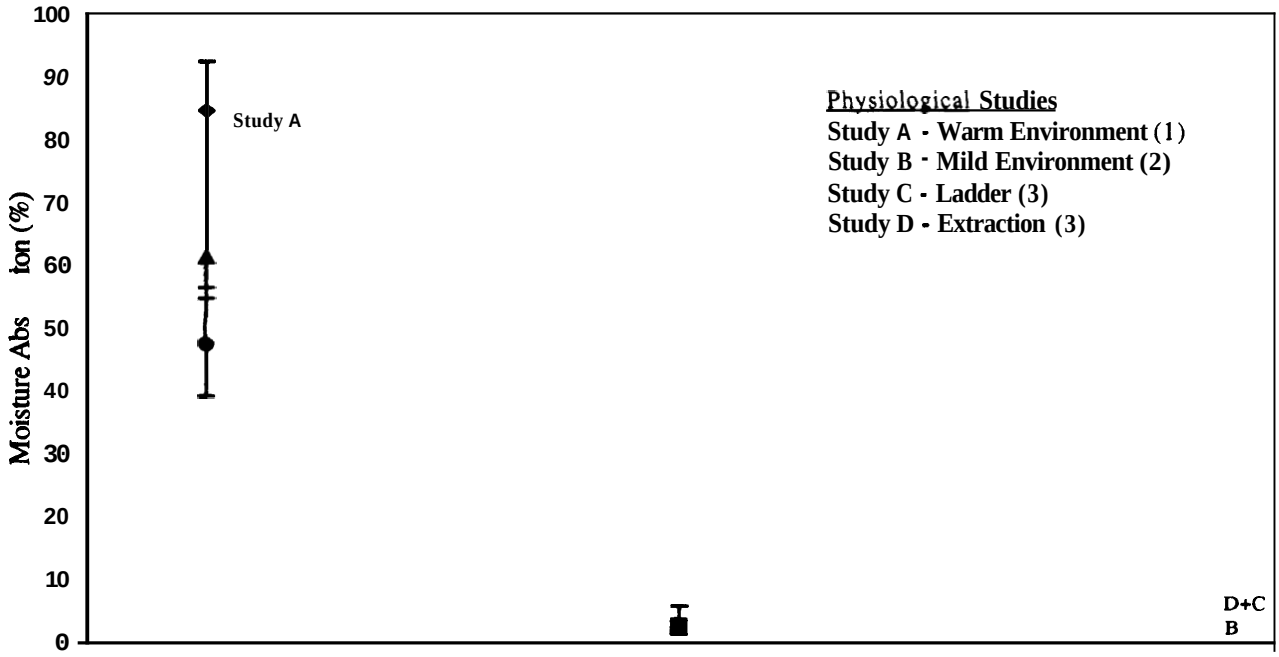

Liauid Sweat Uptake

A modified Gravimetric Absorbency Testing System (GATS) was used to measure the moisture accumulation in turnout composites, simulating the wicking of liquid moisture from direct contact with sweating skin. The GATS procedure measures demand wettablility. The test indicates the lateral wicking ability of the fabric, or the ability of the material to take up liquid in a direction perpendicular to the fabric surface. The NCSU GATS apparatus was modified to incorporate a special test cell and cover to assess absorption behavior in the presence of evaporation (Figure 3).

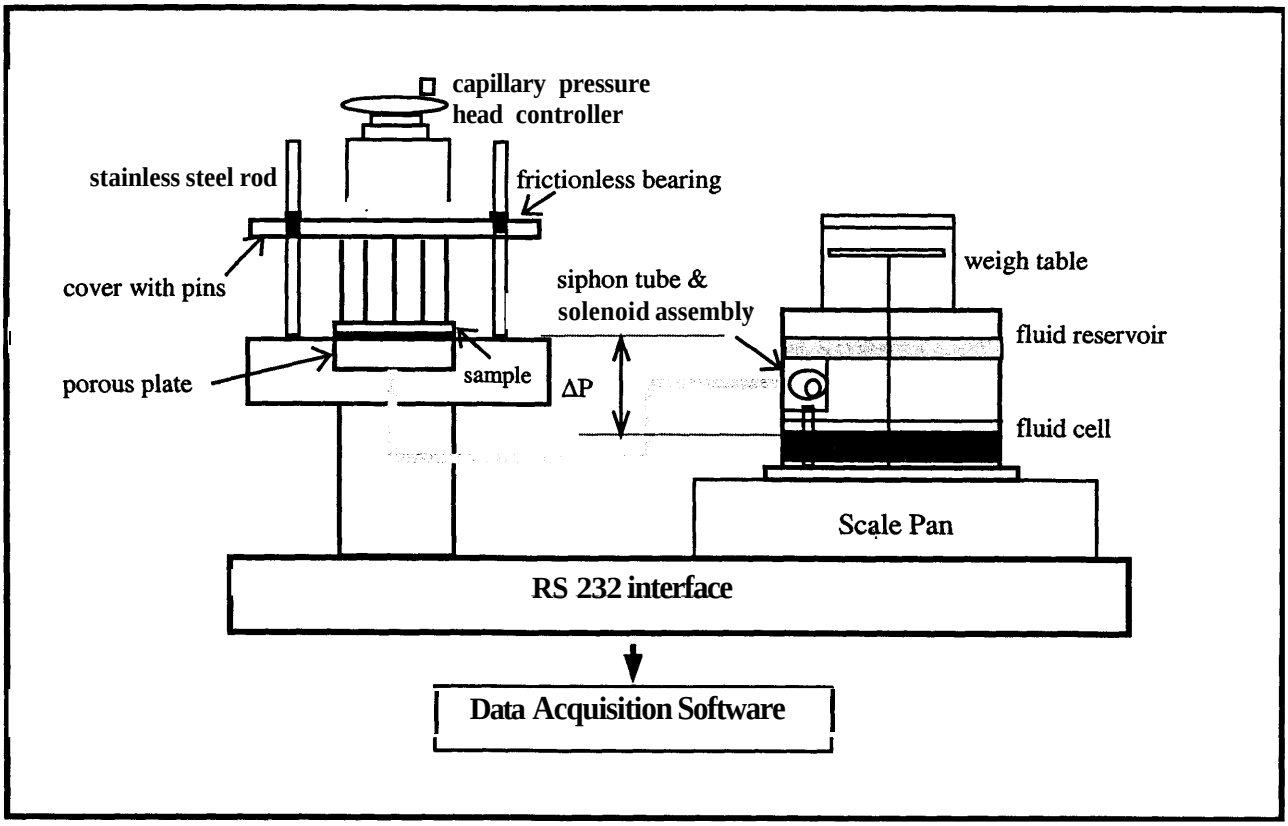

Figure 3. GATS Apparatus

In this arrangement, liquid is drawn from a fluid reservoir by the capillary action of the fabric. The hydrostatic pressure of the fluid delivery system is adjusted by controlling the position of the simple platform (the test is nominally operational with a zero hydrostatic head). Liquid is delivered to the test material placed on a porous plate. Fifty-four pens, distributed over the area of the test surface, uniformly restrain the test fabric. The amount (grams) of liquid siphoned from the reservoir is recorded as a function of time. These data are used to calculate absorption rates, absorption capacities, evaporation capacities, and the percentage of moisture evaporated by the fabric. The GATS was used to measure the uptake of liquid moisture by four different firefighter turnout systems (each liner system was layered with a 7.5 oz/yd^2 Kevlar®/ PBI shell fabric). Results of these experiments are presented in Figures 4 - 6.

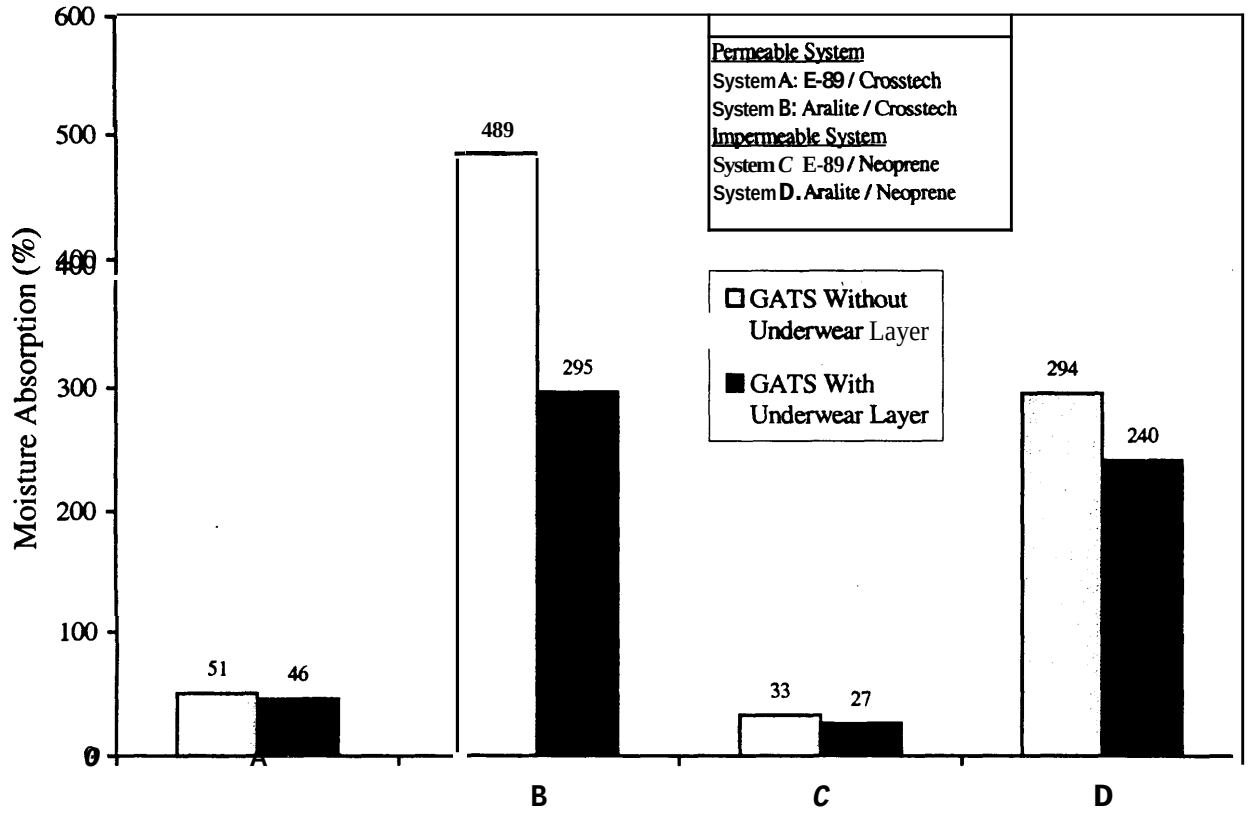

Figure 4. Moisture Absorbed by Turnout Liner Systems (Moisture Barrier/ Thermal Liner) in **CATS**

These data show that the absorption capacity of the thermal liner component is the dominating factor controlling moisture uptake by wicking into the layered turnout composite. We note that liquid moisture uptake by wicking into Aralite® is almost ten times greater than in the E-89® thennal liner. In contrast, since it controls moisture loss by evaporative mechanisms, which is a small fraction of the moisture movement in comparison to wicking, the vapor permeability of the moisture barrier component has much less effect on the liquid pick-up: Breathable moisture barriers (Crosstech®) contribute to less build up of moisture in the thermal liner than the impermeable moisture barrier (neoprene). The effect of moisture barrier permeability is evident in systems that incorporate Aralite® thermal liners. However, while the amount of moisture absorbed and retained in the liner is greatest for nonbreathable composites, Figures **5** and 6 show that the total amount of moisture transported through permeable Crosstech® barriers, over time, approaches the amount absorbed by nonpermeable neoprene systems. These results demonstrate that moisture is also transmitted by evaporation, in breathable turnout systems. Most significantly, these data show that liquid moisture can produce moisture pick-up levels exceeding several times saturation **in** some liners (e.g. the Aralite® systems).

Experiments were conducted to simulate two types of clothing configurations: In one arrangement, the thermal liner was in direct contact with the simulated sweat wetted surface of the **GATS.** In another, absorbent t-shirt and stations uniform clothing layers were placed

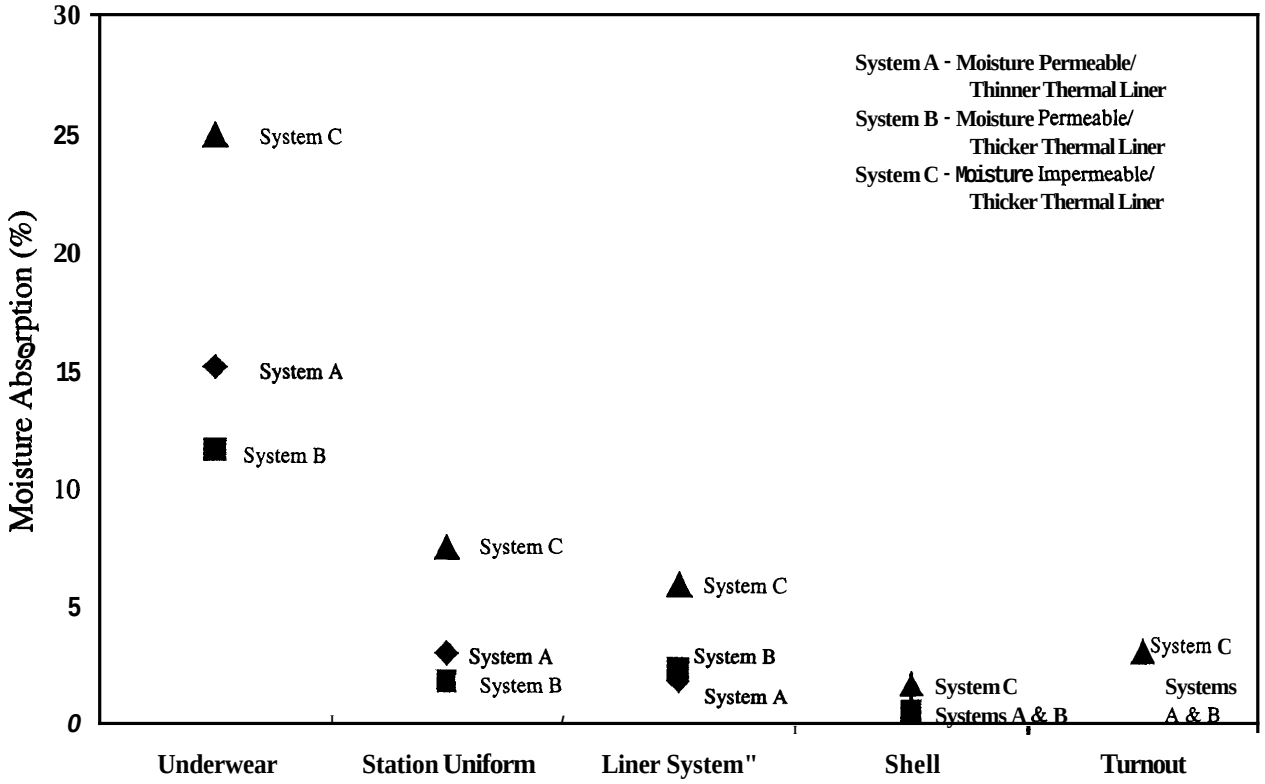

Figure 2. Effect of .Moisture Barrier Permeability and Thermal Liner an Sweat Accumulation in Firefighter Clothing in Wear (Mild Environment Study[2])

*Thermal liner and moisture barrier

Turnout systems that use vapor impermeable moisture barriers generally produce more moisture in inner (t-shirt) clothing layers because there is no opportunity for moisture to escape by evaporation (Figure *2).*

Examination of data from physiological studies provides a first estimate of the amounts and distribution of moisture in firefighter turnouts. This information also gives useful insights into mechanisms of moisture transport in firefighter turnout systems.

Moisture Transport Mechanisms in Turnouts

This research used sophisticated laboratory moisture delivery systems to study ways in which moisture is absorbed and transported in turnout composites. In this regard, moisture is transferred in turnout materials by two basic mechanisms: by wicking of liquid moisture into clothing materials through direct contact with sweat wetted skin, or by condensation of moisture vapor from evaporated sweat.

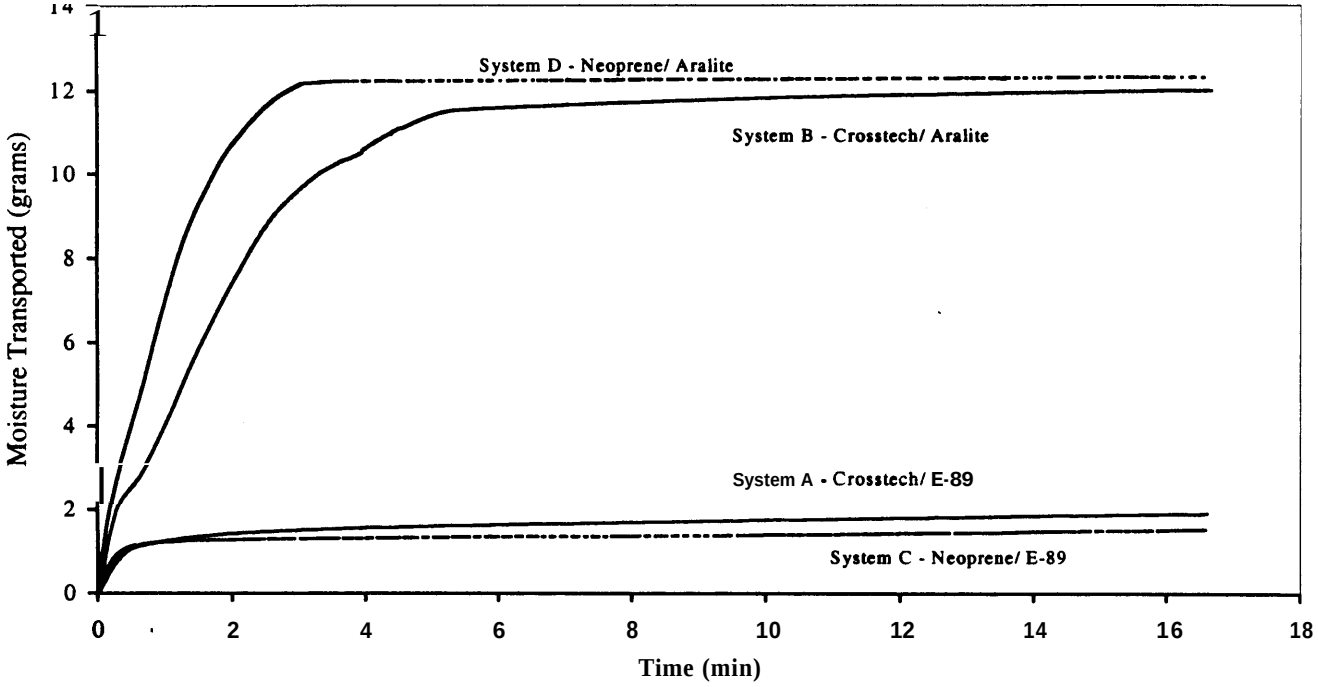

Figure 5. Moisture Transport (Absorbed and Evaporated) by Clothing Systems, Without Inner Clothing Layers, in GATS' as Function of Time.

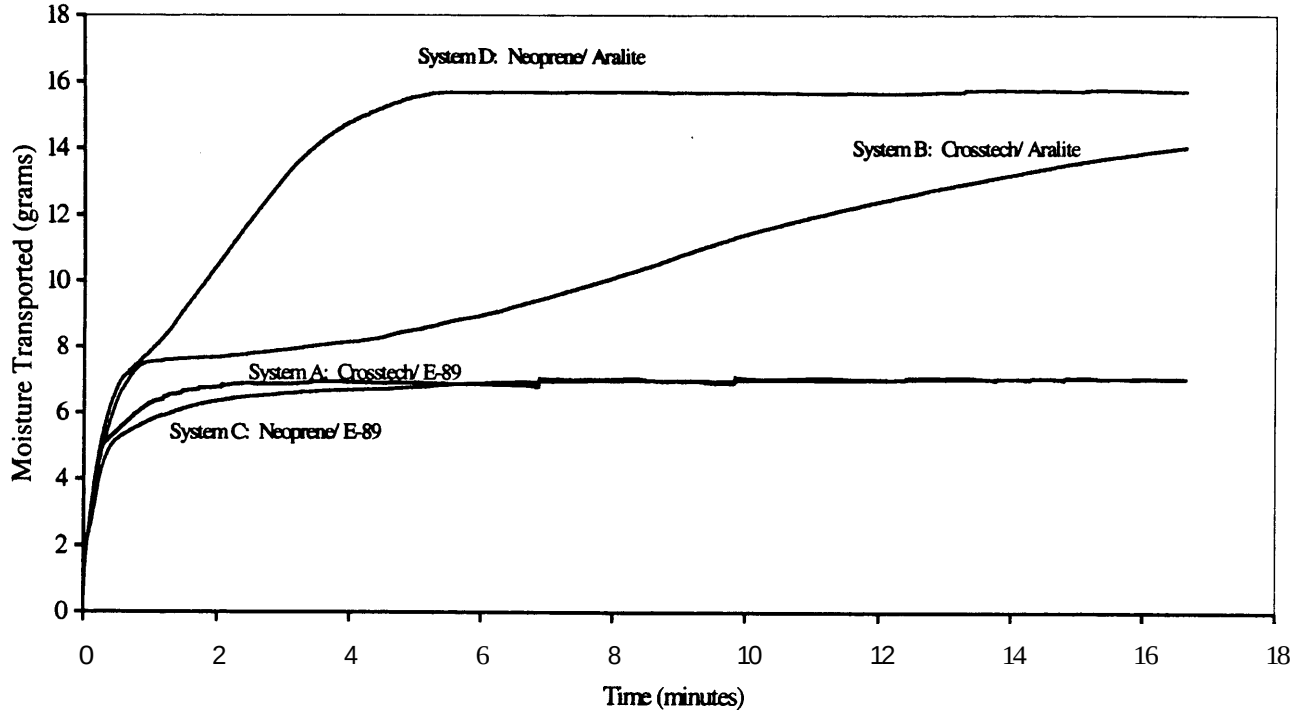

Figure 6. Moisture Transport (Absorbed and Evaporated) by Clothing Systems and Inner Clothing Layers (Underwear and Station Univorm) in GATS as Function of Time.

between the sweat wetted surface and the thermal liner of the turnout composites. Tests show that absorbent clothing inner layers reduce the amount of liquid moisture absorption into the liner system (Figure **4).** However, moisture pick up continues to exceed saturation levels in Aralite® liner systems. These findings suggest that moisture is transported by wicking mechanisms that occur as the intervening absorbent inner layers exceed their saturation capacity.

Moisture Condensation by Sweat Evaporation

A source of moisture accumulation in turnout systems is the condensation of vapor produced by sweat evaporation. Moisture condensation in turnouts is related to the moisture vapor permeability of the turnout and to the transmission of thermal energy. The guarded sweating hot plate (skin model) apparatus, available at NCSU, was used to study this phenomena in firefighter turnout systems. The main component of the skin model is a perforated plate of sintered metal (stainless steel) sized 20 **x** 20 inches (Figure 7).

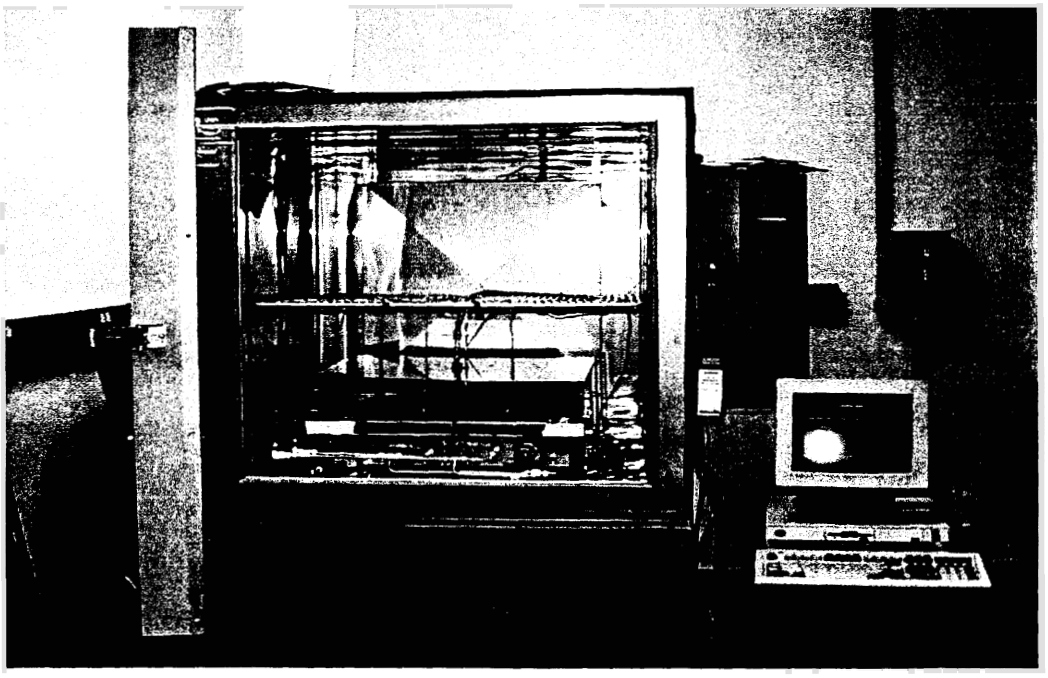

Figure 7. NCSU Sweating Hot Plate Apparatus.

The plate is electrically heated to skin temperature (35° C) and covered by the test fabric. A guard ring heated to the same temperature as the metal plate prevents lateral heat loss. Water is fed from the surface of the test apparatus onto which a cellophane sheet is placed, shielding the fabric form liquid water. The entire assembly is based in an housed in a controlled environmental chamber to provide control of ambient conditions (temperature, humidity) and air flow.

The guarded sweating hot plate apparatus is routinely used to measure heat transfer through clothing materials associated with thermal comfort or heat stress. In this research, it was employed as a controlled moisture delivery system to simulate the process of moisture accumulation in turnouts resulting from vapor condensation. Moisture accumulation from simulated sweat evaporation was determined for four different turnout composite systems. Turnout systems were selected to study effects associated with differences in thermal liners and moisture barriers. The results of these experiments (Figure 8) indicate that the moisture barrier component is the primary source of differences in moisture uptake: for permeable systems (Crosstech®), equivalent amounts of moisture accumulates in E-89® (System A) liner and in the Aralite® liner (System B). On the other hand, because moisture loss by evaporation is prevented in impermeable systems, more moisture builds up in the Aralite® liner than in the E-89® system (Systems C and D).

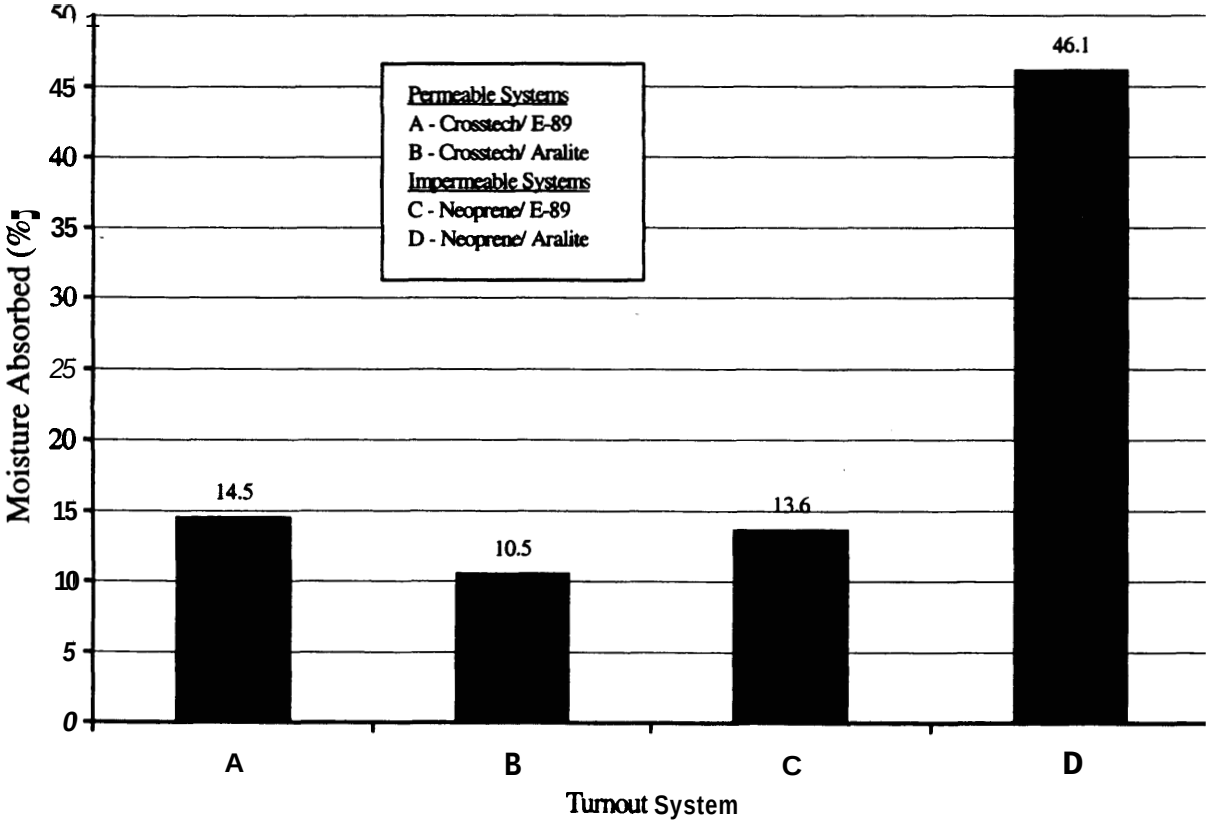

Figure 8. Moisture Absorbed in Turnout Liner (Moisture Barrier/ Thermal Liner) Systems in Sweating Hot Plate (1/2 hour preconditioning at 25 deg C, 65% RH ambient conditions).

Correlations with Sweat Absorption

Comparisons between sweat pick up in turnout systems in actual firefighter wear (Figures 1 and 2), and laboratory experiments that simulate moisture delivery, either by a sweat wicking mechanism or by condensation of evaporative moisture, indicate that moisture levels are most closely approximated by laboratory preconditioning with the guarded sweating hot plate. Sweating plate preconditioning, that used absorbent inner layers, can be expected to produce closer correlation with moisture levels observed in wear. These results suggest that, when thermal liners do not directly contact liquid sweat, and the level of moisture in inner clothing layers is less than saturation level, moisture accumulates by condensation of evaporated moisture vapor. Moisture build up by processes involving the wicking of liquid sweat can be expected in cases where the thermal liner is in intimate contact with sweat wet skin, as simulated by the GATS procedure.

Developing a Practical Preconditioning Procedure

The described studies provide valuable insights into the mechanisms of moisture transport in firefighter turnout systems. They show that moisture can accumulate in turnouts, both by wicking of liquid moisture, and by condensation of evaporated sweat. They demonstrate that the level, and distribution of absorbed moisture, varies depending on the type of thermal liner, the breathability of the moisture barrier component, and on the presence of underlying absorbent clothing layers. This knowledge can now be applied to develop rational preconditioning protocols for evaluating the effects of moisture on thermal protective performance in prolonged exposure to radiant heat. In this regard, our experiments suggest that the sweating guarded hot plate may be a means of preconditioning turnouts to realistic levels of moisture content prior to thermal testing. However, the sweating plate procedure involves the use of elaborate and costly laboratory equipment and, therefore, may not be ideal as a practical preconditioning method. Consequently, the following simpler procedure was adopted: The turnout test specimen is precisely weighed. Sufficient water is then sprayed onto the facecloth side of the thermal liner to increase the weight of the turnout composite (thermal liner, moisture barrier, shell fabric) by approximately 15 percent. This amount of add-on was chosen to reasonably approximate the level of moisture actually absorbed by turnout liners, as observed in wear trials (see Figure 1). The turnout composite is sealed in a plastic bag and allowed to condition for a period of at least twelve hours. Specimens are subsequently removed from the sealed bag and precisely weighed.

Table 1 shows the results of triplicate determinations on four different turnout materials. These data confirm that the above described moisture preconditioning protocol produces consistent amounts of moisture add-ons, with little variability in repeated tests. The demonstrated consistency of the protocol is a significant development, since it has been shown that reproducibility of moisture effects on thermal tests is critically controlled by the ability to consistently load moisture into test specimens [4].

An additional characteristic of the moisture preconditioning protocol is illustrated in Figure 9.

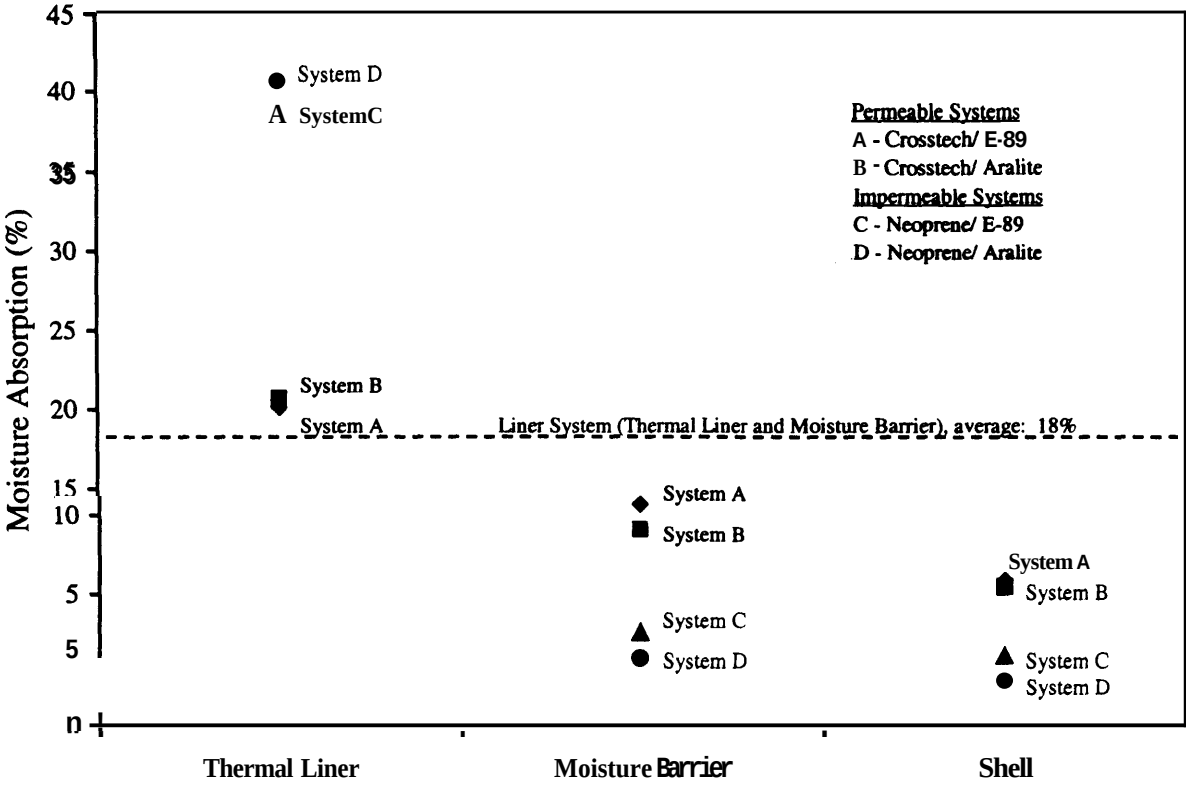

Figure 9. Distribution of Moisture in Turnout Layers
Using Laboratory Protocol

These results demonstrate that the procedure results in the highest accumulation in the thermal liner, the innermost component of the turnout system. Significantly less moisture accumulates in the moisture barrier and shell fabric. Therefore, the moisture gradient observed mimics the gradient that occurs in actual wear, where clothing layers closest to sweat wetted skin retains the highest percentage of moisture (see Figure 2). The observed consistency of the preconditioning procedure as well as the moisture gradient produced in different layers of the turnouts, are undoubtedly facilitated by the step in the protocol that calls for a lengthy conditioning period in a sealed plastic bag. This step allows moisture distribution to occur within the layers of the turnout specimen.

Moisture from External Sources

A study was conducted to develop a preconditioning protocol to simulate moisture penetration from fire ground sources through the outer shell fabric and components including trim. We studied several test methodologies including a water impact penetration test (AATCC Test Method 42) and a rain test (AATCC Test Method 35). The objective of these experiments was to establish variables in water spray type preconditioning procedures for optimum water exposure to shell and trim components.

Table 1. Moisture Pick-up in Turnout Materials Using Preconditioning Protocol

System* -Replicate	Moisture Pick-up (%)
A: Crosstech®/ E-89	
-1	17.7
-2	18.5
-3	18.1
Average	18.1
% CV	2.3
B: Crosstech®/ Aralite®	
-1	17.4
-2	18.1
-3	18.3
Average	18.0
% CV	2.7
C: Neoprene/ E-89	
-1	19.3
-2	18.1
-3	19.1
Average	18.8
% CV	3.6
D: Neoprene/ Aralite®	
-1	18.3
-2	18.7
-3	18.1
Average	18.4
% CV	1.7

*Each system was layered with a 7.5 oz/yd^2 Kevlar®/ PBI shell fabric.

Water Penetration Tests

We have investigated several standardized test methodologies for exposing fabrics to water spray, including a water impact penetration test (AATCC Test Method 42) and a rain test (AATCC Test Method 35). In both test procedures a turnout shell fabric (7.5 oz/yd^2 Kevlar®/ PBI) was exposed to carefully controlled water sprays. The purpose of these experiments was to determine the amount of water absorbed by the shell fabric itself, and to estimate the amount of water penetrating through a typical turnout shell fabric with and without reflective trim attached to it.

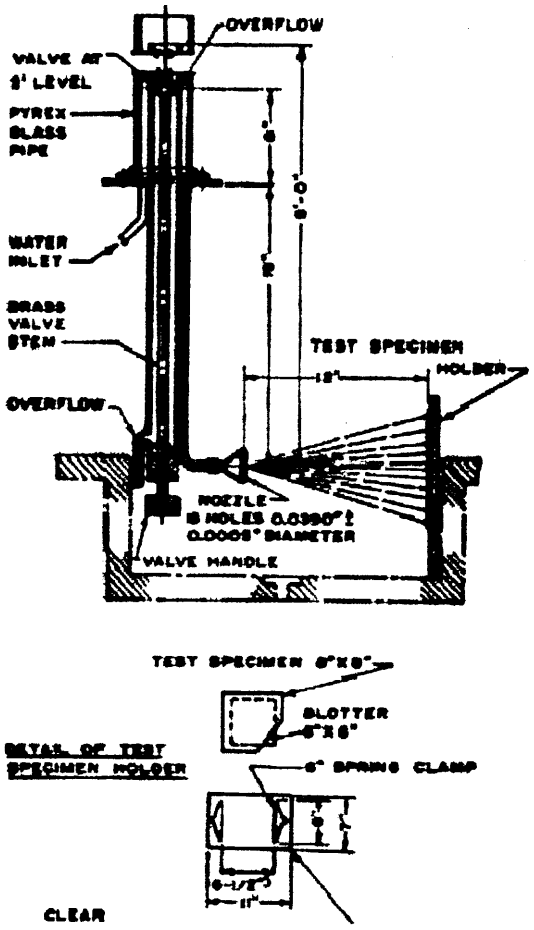

Figure 11. Structural Details of Rain Tester [6].

Figures 12 and 13 show the results of experiments conducted using the above described testing arrangements for spraying water onto the turnout fabric, with and without attached trim.

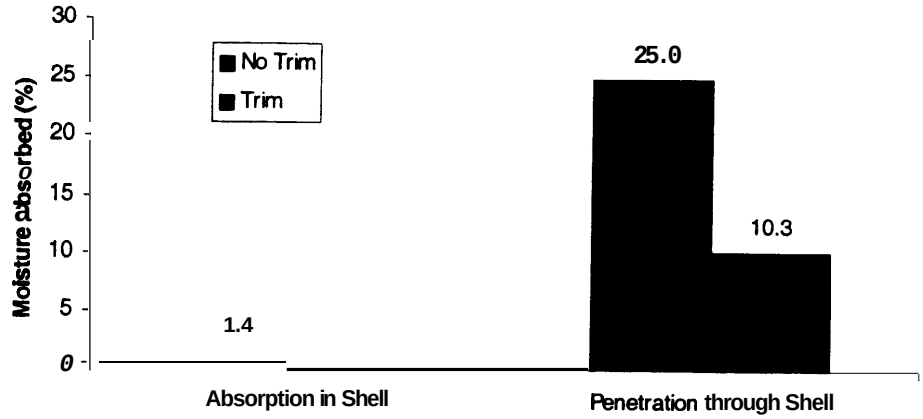

Figure 12. Results of Impact Penetration Test.

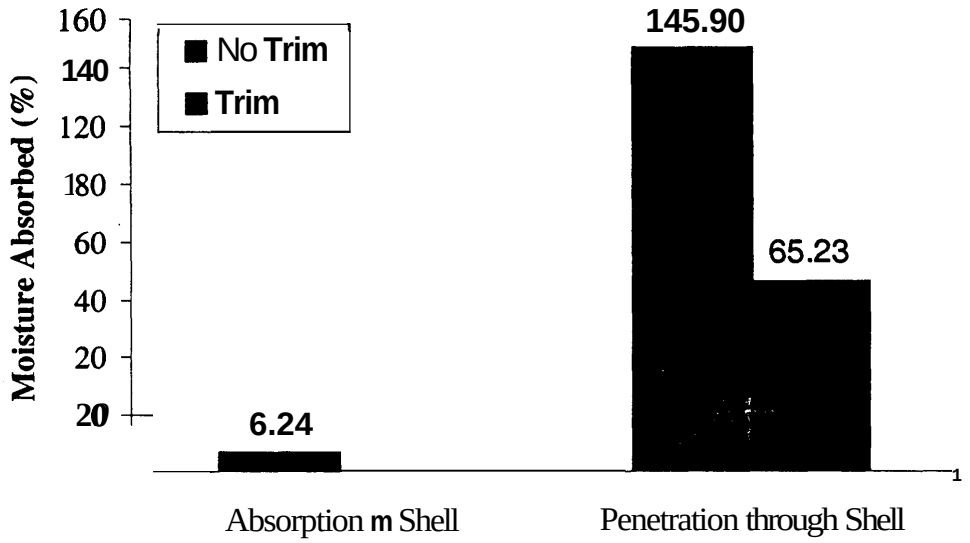

Figure 13. Results of Rain Test

These data indicate that significant amounts of water penetrate the turnout shell fabric, even with reflective trim in place. In turnout composites, this moisture can be expected to accumulate in the outside facing or substrate layer of the moisture barrier. Therefore, these experiments demonstrate that moisture from external sources may, in fact, reside between a vapor impermeable reflective trim component and a vapor permeable moisture barrier, in breathable composites. A primary objective of subsequent research will be to assess the effects of this moisture on heat transfer through turnout materials exposed to low level thermal energy.

Thermal Sensor Technologies

A significant technical barrier to the development of a test method to evaluate thermal protection in low level heat exposures has been the availability and validation of a thermal sensor, and associated bum translation model. The Center for Research on Textile Protection and Comfort (T-PACC) at North Carolina State University has developed thermal sensor technologies which can be advantageously used for this application.

The NCSU Water-cooled Prototype Sensor

The NCSU water-cooled thermal sensor was developed specifically for measuring heat flux in prolonged thermal exposure. The water cooled sensor was designed to overcome limitations related to heat build up characteristic of slug type thermal sensors, such as the TPP sensor. Figure 14 illustrates the design concept for the water cooled sensor.

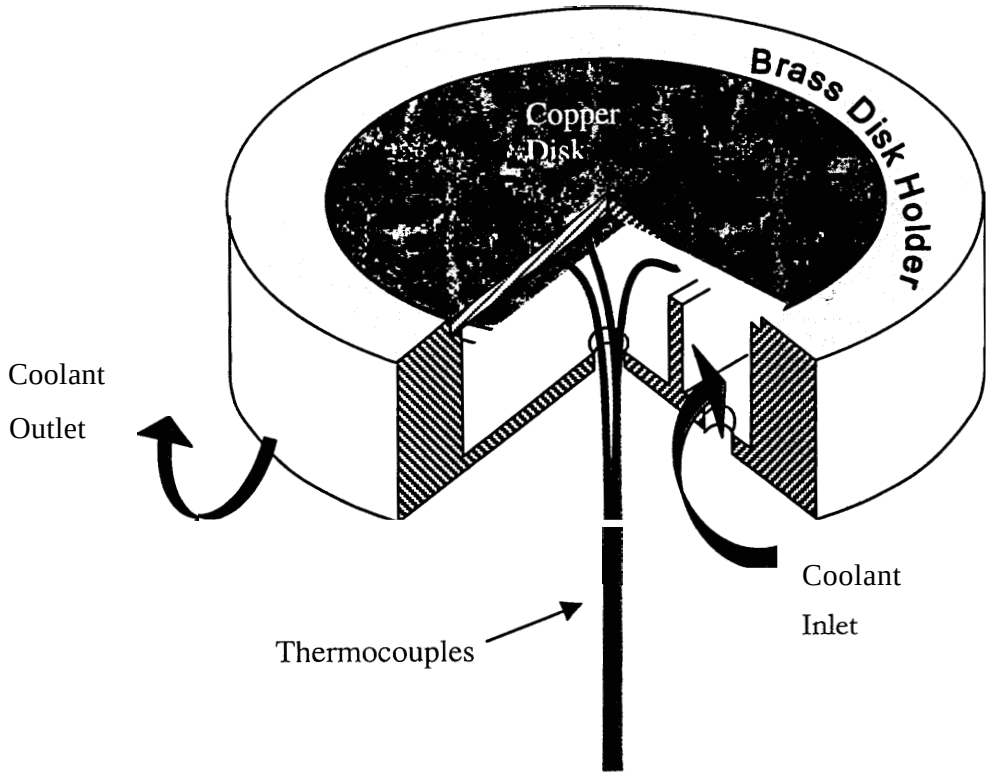

Figure 14. NCSU Water Cooled Sensor

The sensor assesses incident heat flux by measuring the difference between the temperature of the copper slug calorimeter and the water flowing through the system. Details of the computation model can be found in an appendix to this report.

A differential thermal balance equation was used as:

$$\frac{dQ}{dt} = \frac{dm}{dt} Cp\Delta T$$

Where Q is the incident heat flux
AT is differential temperature and
m and Cp are the mass and specific capacity of the water flowing through the sensor.

This principal equation was used to estimate the minimum water flow rate, dm/dt, required by the sensor. Details of the computational model used can be found in Appendix A to this report.

Figure 15 compares the response of the NCSU water cooled and the Hy-Cal Hy-Therm@sensor in direct exposure to a low level heat source (2.5 kw/m^2).

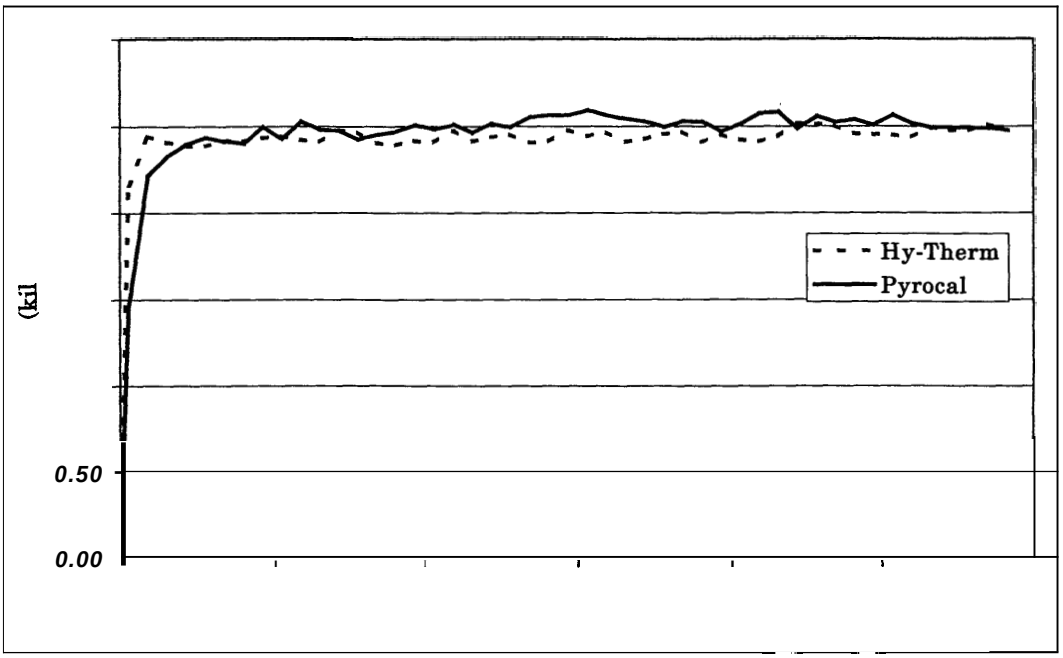

Figure **15.** Direct Exposure to **2.5** kW/m^2 Heat Flux Level.

These data show that the **NCSU** water cooled sensor, while slower to respond to heat, produces stable readings over lengthy exposures, which are comparable to the Hy-Therm® instrument. However, unlike the Hy-Therm, the **NCSU** prototype is a rugged device, with sufficient durability for use in testing thermal protective materials.

Comparing Sensors for TPP Testing

Experiments have been conducted to evaluate four different sensors for measuring the thermal protective performance of firefighter turnout materials in low level heat exposures: NCSU's Pyrocal and Pyrocool water-cooled sensors, the TPP and the Thermoman® sensors. The Pyrocal sensor is extensively described in reference **7.** The TPP thermal sensor is a slug claorimeter widely used to evaluate thermal protective performance in bench scale tests. The Thermoman® sensor is an embedded thermocouple sensor developed for the Thermoman® fire test manikin system.

The RPP test platform was used at test exposures of **6.3** and **9.6** kw/m^2 **(0.15** and **0.23** cal/cm^2·sec). The RPP test apparatus is described in ASTM Test Method F **1939-99,** Standard Test Method for Radiant Protective Performance of Flame Resistant Materials.

Bum Estimates

A crucial question to be addressed is how different sensors, and their associated bum translation criteria, compare in predicting the onset of bum injury in low level heat exposures. Figure 16 shows the second degree bum estimates made using different types of thermal sensors. The Stoll criteria was used to predict time to second degree bum for the TPP, Pyrocal and NCSU water-cooled sensor [*8*, *9*]. The skin model bum translation algorithm used in the Thermoman® manikin was applied for the Thermoman® sensor. This bum model is based on criteria suggested by Henriques [*10*]. Bum predictions obtained from these sensors compared with an estimate based on the temperature registered by a thermocouple attached to the innermost thermal liner fabric of the turnout composite. In this case a criteria used in recent work by NIST and 3M was applied: the innermost fabric surface temperature of **55°C** is used as an indication of the potential for second degree bum [*11*].

The results in Figure 16 show that the TPP and Thermoman® sensors give the highest bum prediction times: The TPP sensor predicts no bum at the lowest exposure level (6.3 kw/m^2). The bum prediction times are two times greater for the Thermoman® sensor than for the Pyrocal or Pyrocool sensors. The difference in the bum times predicted by different sensors can be partially explained by examining the response over the duration of the exposure (Figures **17** and 18). These data indicate that, in comparison to the water cooled (Pyrocool) and Pyrocal sensors, the heat flux read by the TPP sensor is observed to drop off during the lengthy thermal exposure. This tendency is also observed in the Thermoman® embedded thermocouple sensor, although the deterioration in the flux reading is not nearly as pronounced as observed with the **TPP** sensor. Both the calorimeter type (TPP) and thermcouple (Thermoman®) sensors are constructed of materials that retain thermal energy during the exposure sequence. Subsequently, the sensor's internal temperature rises to levels that make the sensor unable to accurately differentiate incident heat flux. To a certain extent, all of these type sensors become impaired at long durations. Heat storage effects are circumvented in the Pyrocal thermal sensor using a computation method to account for heat losses from the copper disk. The computational adjustment procedure is described in Appendix B to this report and in reference 7.

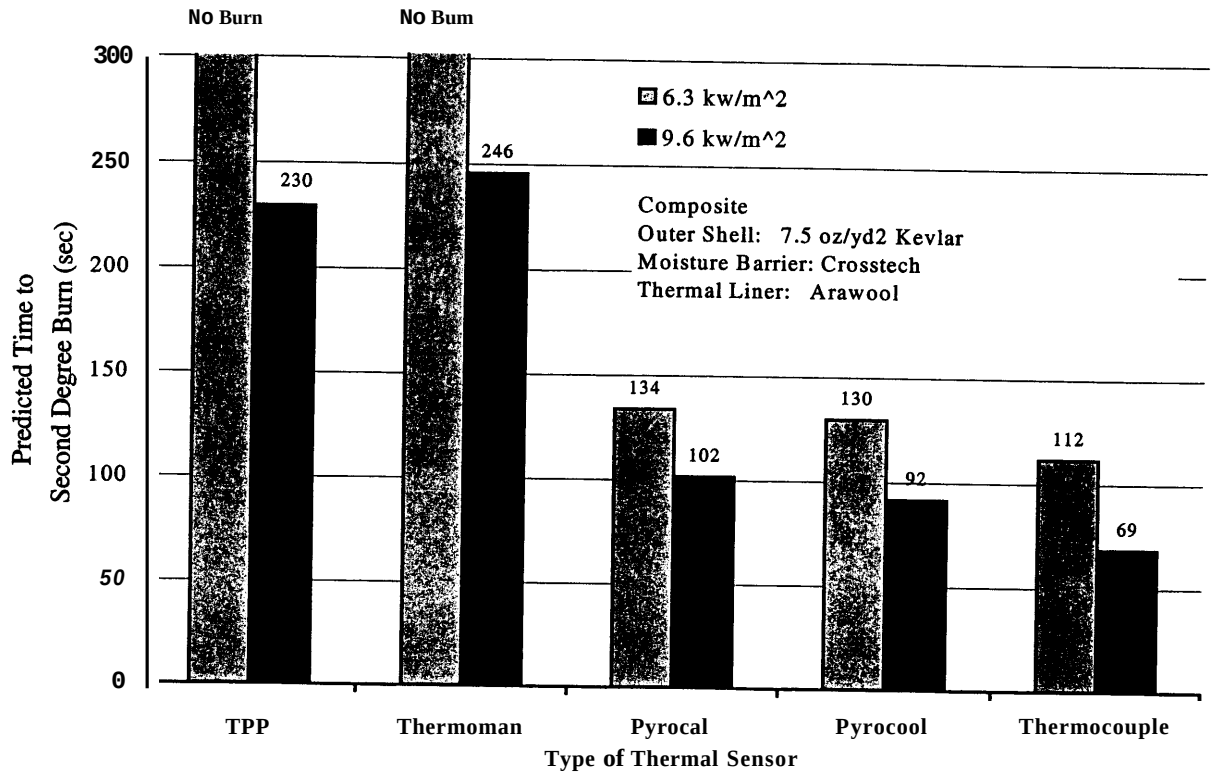

Figure 16. Comparison of Burn Prediction Times Using Different Thermal Sensors

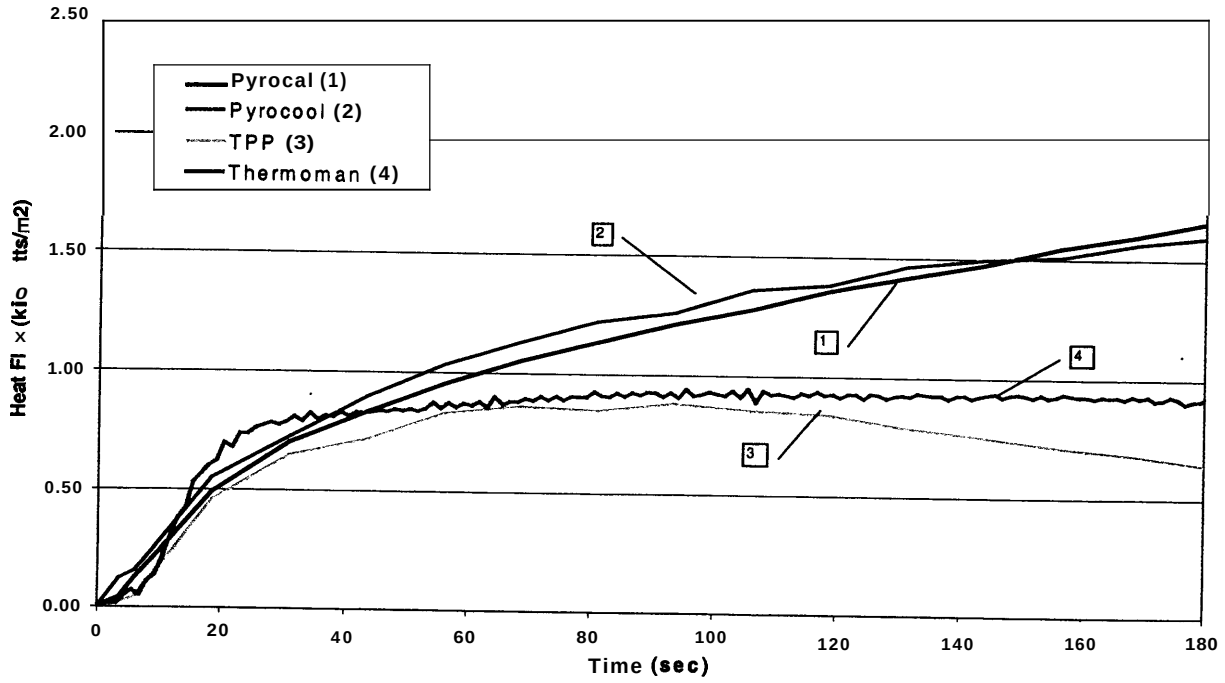

Figure 17. RPP Exposure at 6.3 kW/m^2 Heat Flux Level.

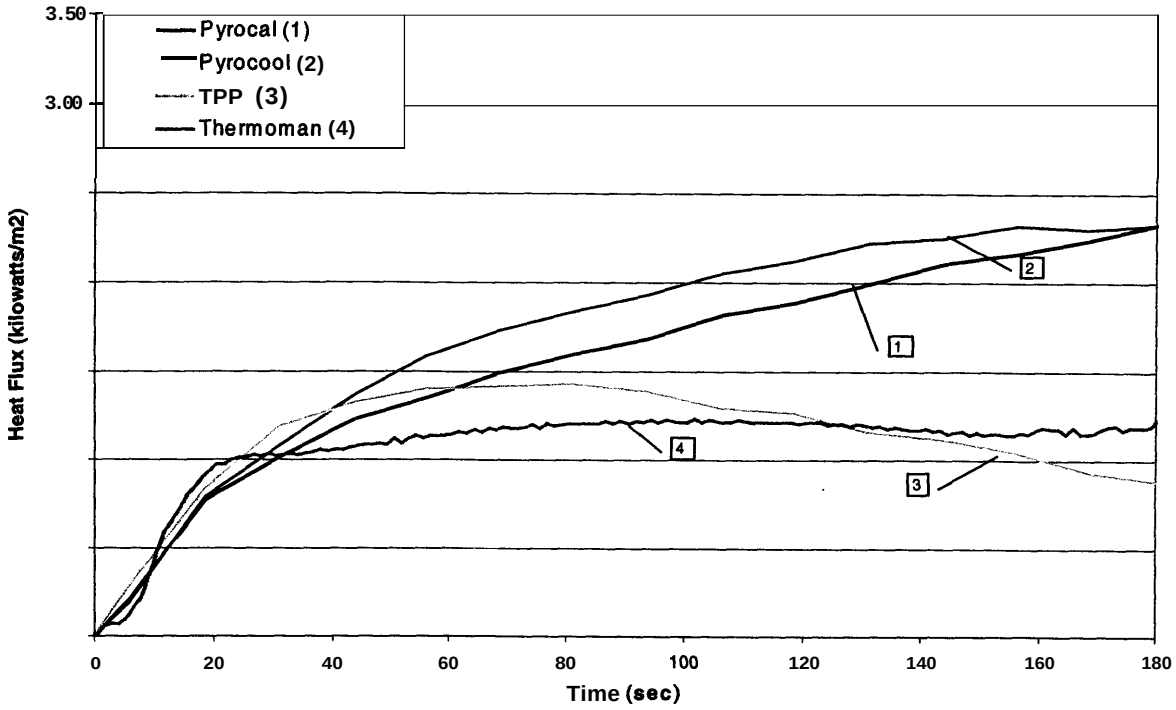

Figure 18. RPP Exposure at 9.6 kW/m2 Heat Flux Level

The prediction based on thermocouple readings of the innermost fabric surface temperature is observed to provide the fastest estimate of bum time, especially at the highest thermal exposure (Figure 16). These findings are consistent with those previously reported by Neal [*12*]. They indicate possible cautions that may apply in using simple measurement of fabric surface temperature as a basis for predicting skin bum injury.

Moisture Effects in **LOW** Level Heat Exposures

Experiments have been initiated to study the effects of moisture on the thermal protective performance of firefighter turnout composites in low level thermal exposures. The arrangement shown in Figure 19 was used to expose a turnout composite, consisting of a 7.5 oz/yd^2 Kevlar®/ PBI outer shell, Crosstech® on Nomex® pajama check moisture barrier and Aralite® thermal liner, to heat exposures ranging from 6.3 to 21 kw/m^2 (0.15 to 0.5 cal/cm^2·sec) in intensity.

The heat source consists of a bank of quartz tubes positioned directly below the test sample. Transmitted heat flux was measured using the Pyrocal sensor, and these measurements are used to estimate the time to second degree bum, based on the Stoll criterion [*9*]. An extrapolation of the Stoll criterion was used to estimate time, since predicted time to second degree burn exceeded 30 seconds (See Appendix B to this report). Multiple thermocouples, positioned between the shell fabric and moisture barrier, and between the moisture barrier and thennal liner, and on the innermost (face cloth) side of the thermal liner, measured the temperature gradient across individual fabric layers of the turnout system.

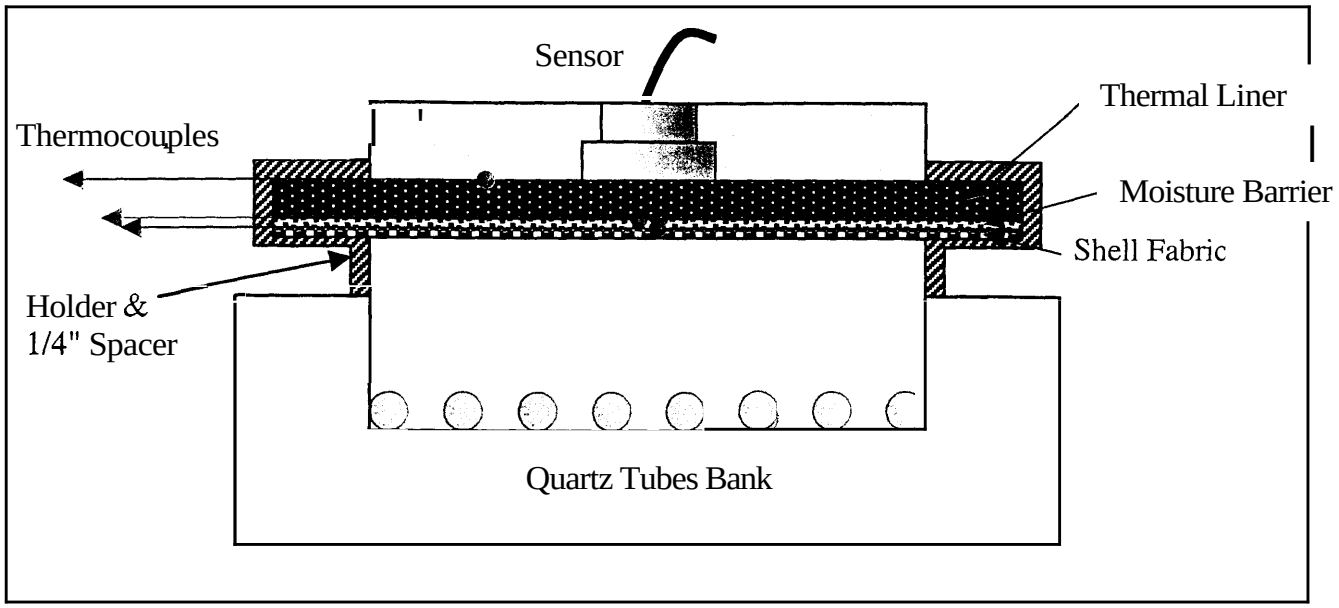

Figure 19. Apparatus used in Thermal Tests

The following moisture preconditioning protocol was followed: sufficient water was sprayed directly onto the face cloth side of the thennal liner to achieve 100%add on, based on the dry weight of the turnout composite (approximately 16 grams of water). The turnout system was subsequently sealed in a zip lock bag. Test samples were allowed to equilibrate for at least twelve hours prior to thermal testing. The distribution of moisture in the different layers of turnout composites, preconditioned in this manner, is shown in Figure 20.

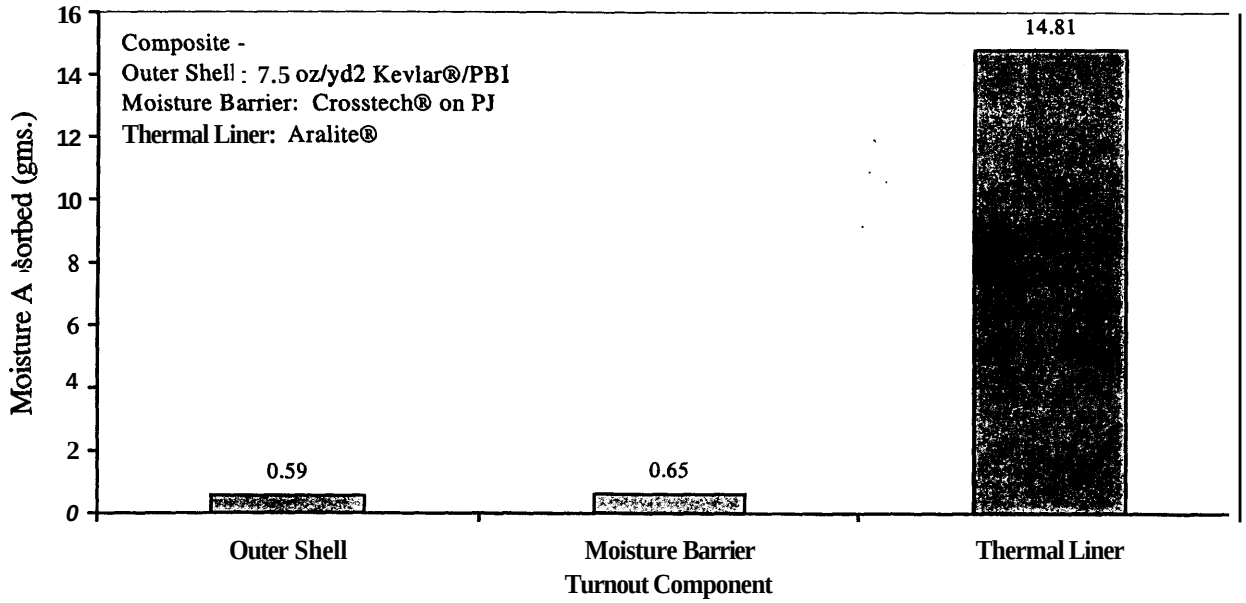

Figure **20.** Moisture Distribution in Turnout System

These data indicate that moisture is distributed throughout the layers of the test composite; however, most of the moisture resides in the thermal liner component.

Test results, showing the effects of saturation level moisture on predicted second degree bum time, at different heat exposure levels, are shown in Figure **21.**

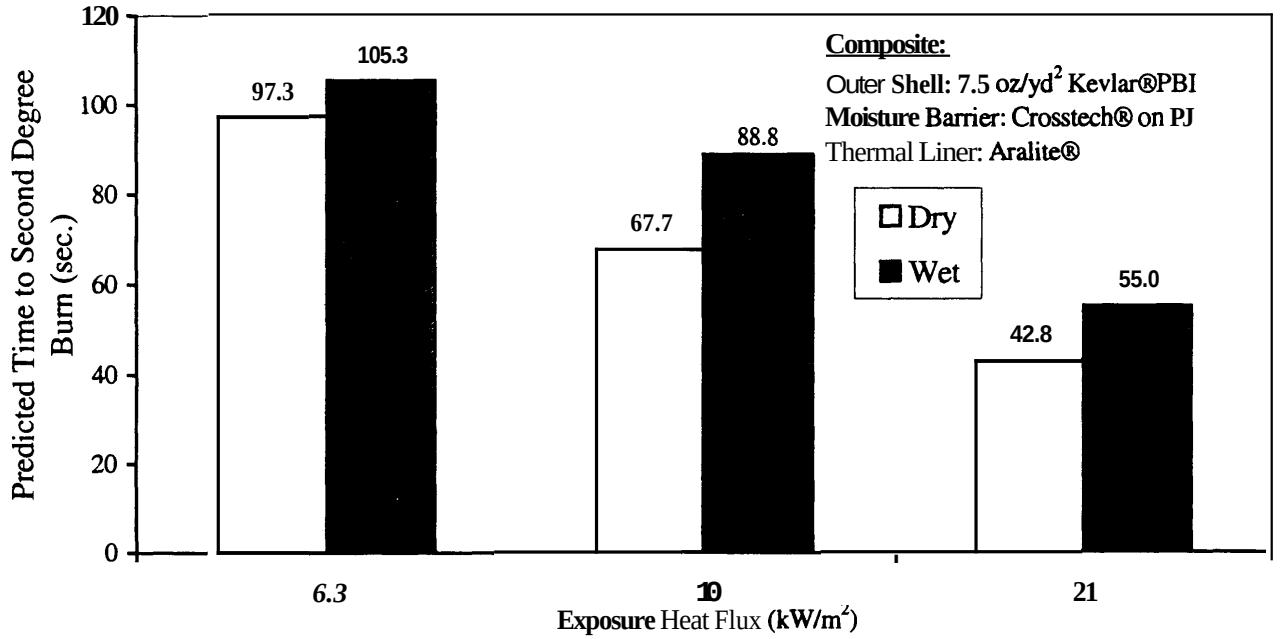

Figure **21.** Effect of Moisture on Predicted Time-To-Bum in a Vapor Permeable Turnout System

These results show a predictable diminishment in thermal protection as the intensity of the heat exposure increases. Most significantly, they show that, preconditioned as indicated above, moisture acts to increase the thermal protective performance of this vapor permeable turnout sample. Instrumented thermal measurements, shown in Figures **22** and **23,** provide explanation of these findings.

Thermal transfer through the dry and moisture preconditioned sample clearly indicates the effect that moisture has in reducing transmitted heat energy. These effects are undoubtedly due to energy absorbed in heating moisture residing in fabric layers, and the resulting effect on reducing temperature buildup in the turnout system.

Observed inflections in the heat transfer and temperature curves (Figures **22** and **23) are** indicative of moisture heating and phase transitions effects and the impact of these phenomena on heat buildup and transmission. These are obviously complex phenomena determined by interrelated factors including the insulation and vapor permeability of the turnout composite, moisture and temperature distribution in individual layers, and by the intensity of the heat

exposure. These transfer phenomena, including the effects of vapor impermeable moisture barriers and trim, are subjects of our extensive and ongoing investigation.

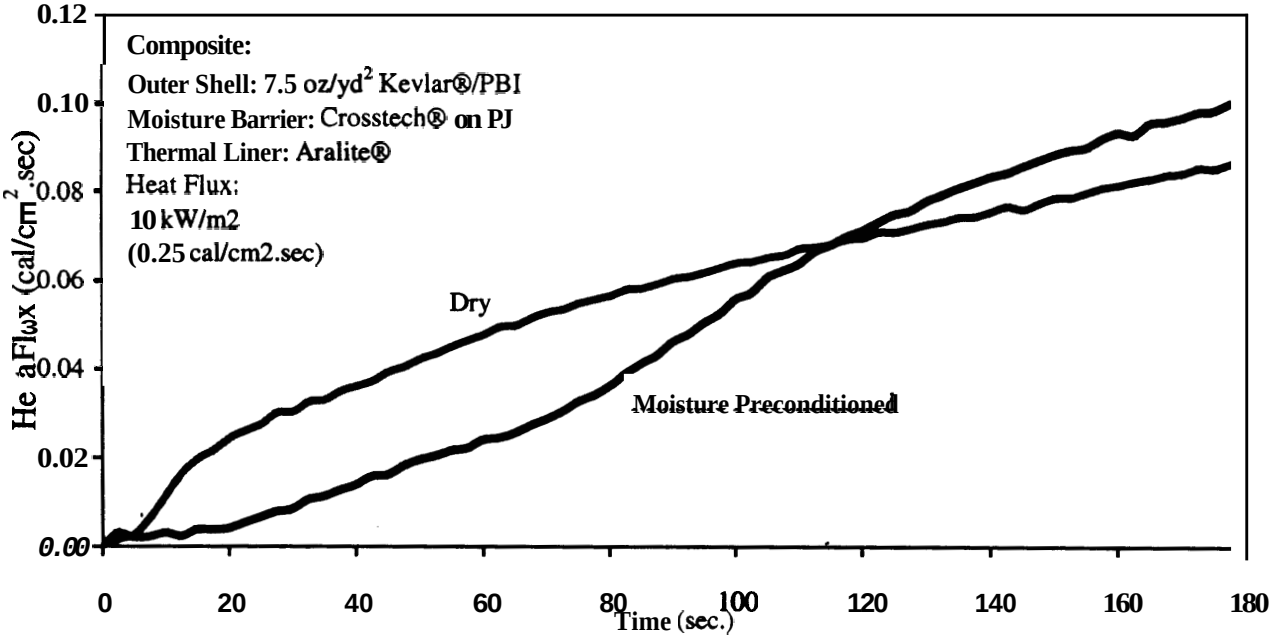

Figure 22. Heat Transfer Through Dry and Moisture Preconditioned Turnout System

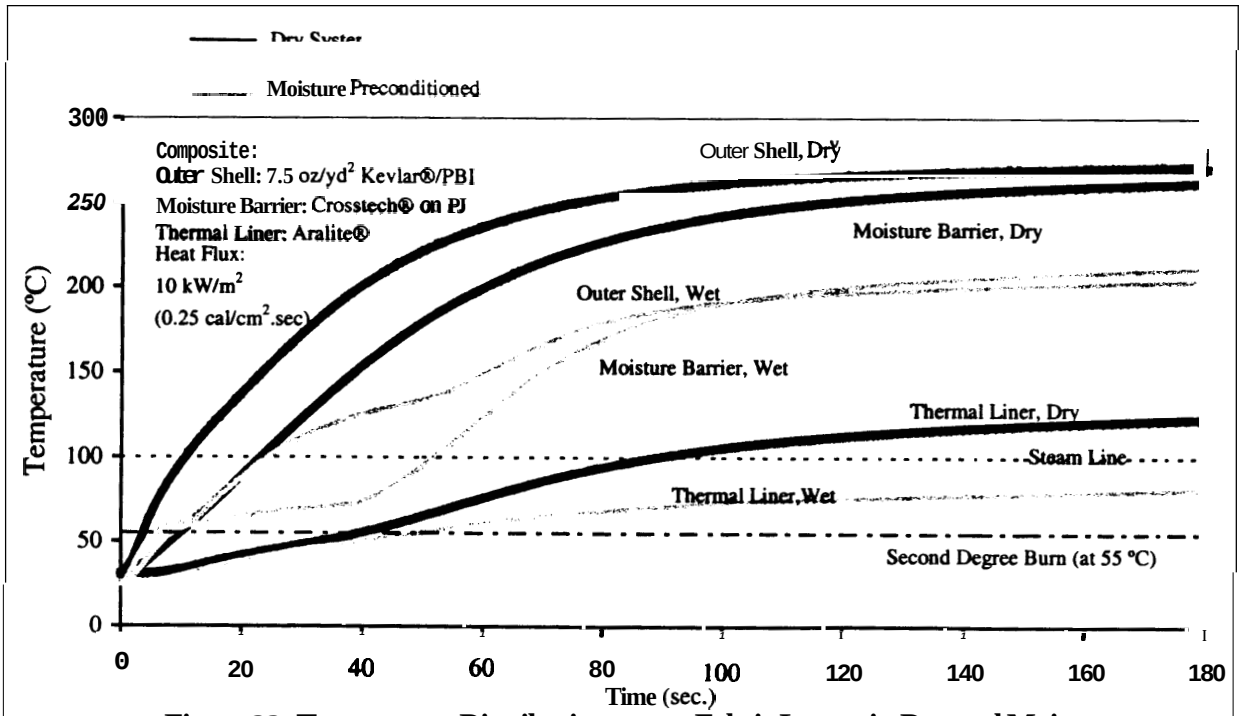

Figure 23. Temperature Distribution across Fabric Layers in Dry and Moisture Preconditioned Turnout Systems

Follow-on Work

The second year of this project will be devoted to the following tasks:

- Validation of the moisture preconditioning protocol. This research has shown that water soaking and vapor saturation (greenhouse) methods provide promising means of consistently introducing moisture into turnout composites in a way that simulates accumulation by condensation of evaporated sweat. Continued effort will be made to confirm the utility of this technique for a variety of different types of turnout systems and for different levels of moisture loading.

- This research has demonstrated the potential value of the Pyrocal and Pyrocool sensors for low level heat tests. However, assessments thus far have been based on limited number of experiments involving a single type of turnout composite. Additional sensor studies will be made, therefore, to confirm results and to include tests on a wider range of turnout materials, with and without moisture introduced into the test composites.

- Full analysis of moisture effects on bum potential over a range of low level heat exposures. Systematically designed experiments will be performed to study the effect of composition, absorption and permeability of shell, moisture barrier, thermal liner and trim components on moisture related effects on thermal protective performance. The developed moisture preconditioning procedures will be used to introduce different loads and distributions of moisture into the test turnout systems. Thermal exposures ranging from 6.3 to 21 kw/m^2 (0.15 to 0.5 $cal/cm^2 \cdot sec$) will be generated using a radiant panel platform. We expect to work closely with personnel at the Building and Fire Research Laboratory (BFRL) at NIST to complete the scientific and practical objectives of the program.

References

1. Myhre, L. G., Barker, R.L., Scruggs, B.J., Shalev, I., Prahsam, C., and Miszko, T., "Effect of Measured Heat Loss Through Turnout Materials on Firefighter Comfort and Heat Stress. Part II: Performance in a Warm Environment," ***Perfomnce of Protective Clothing: Issues and Priorities for the 21st Century: Seventh Volume ASTM STP 1386,*** C.N. Nelson and N.W. Henry, Eds., American Society for Testing and Materials, West Conshohocken, PA, 2000 (In Press).

2. Barker, R.L., Myhre, L.G., Scruggs, B.J., Shalev, I., Prahsam, C., and Miszko, T., "Effect of Measured Heat Loss Through Turnout Materials on Firefighter Comfort and Heat Stress. Part I: Performance in a Mild Environment," ***Perfomnce of Protective Clothing: Issues and Priorities for the 21st Century: Seventh Volume ASTM STP 1386,*** C.N. Nelson and N.W. Henry, Eds., American Society for Testing and Materials, West Conshohocken, PA, 2000 (In Press).

3. Stull, J. O., Duffy, R. M., "Field Evaluation of Protective Clothing Effects on Fire Fighter Physiology: Predictive Capability of Total Heat Loss Test," ***Performance of Protective***

Clothing: Issues and Priorities for the 21st Century: Seventh Volume ASTM STP 1386, C.N. Nelson and N.W. Henry, Eds., American Society for Testing and Materials, West Conshohocken, PA 2000 (In Press).

4. Barker, R. L., Guerth, C., Behnke, W. P., and Bender, M., "Measuring the Thermal Energy Stored in Firefighter Protective Clothing," ***Performance of Protective Clothing: Issues and Priorities for the 21st Century: Seventh Volume ASTM STP 1386,*** C.N. Nelson and N.W. Henry, Eds., American Society for Testing and Materials, West Conshohocken, PA, 2000 (In Press).

5. AATCC Test Method **42,** Water Resistance: Impact Penetration Test, AATCC, Research Triangle Park, NC.

6. AATCC Test Method 35, Water Resistance: Rain Test, AATCC, Research Triangle Park, NC.

7. Grimes, R., Mulligan, J.C., Hamouda, H., and Barker, R. "The Design of a Surface Heat Flux Transducer for Use in Fabric Thermal Protection Testing;" Performance of Protective Clothing: Fifth Volume, ASTM STP 1237. James **S.** Johnson and S.Z. Mansdorf, Eds. American Society for Testing and Materials. West Conshohocken, PA. **1966,** pp. **607 - 624.**

8. Stoll, A. M., and Chianta, M. A., "Method and Rating Systems for Evaluations of Thermal Protection," Aerospace Medicine, Volume **40 (1969).**

9. Stoll, A. M., and Chianta, M. **A.,, "Heat** Transfer Through Fabrics **as** Related to Thermal Injury," Transactions - New **York** Academy of Sciences, Vol. 33 **(7), (1971).**

10. Henriques, F. ***C.,*** "Studies of Thermal Injury: V. The Predictability and the Significance of Thermally Induced Rate Processes Leading to Irreversible Epidermal Injury," Archives of Pathology, Vol. **43,** p. **489, 1947.**

11. Jensen, R. L., Jr., "Thermal Performance of Fire Fighters' Protective Clothing," Safety and Security Systems Division, 3M Center, Building **225-4N-14,** St. Paul, MN **55144-1000.**

12. Neal, **T.** E., "Prediction of Fire Fighter Bum Injury Using Skin Model Sensors at Low Level Heat Exposures, Preliminary Results from DuPont," presented at the Meeting of **NFPA 1971** Technical Committee, Portland, Maine (July **1998).**

Appendix A

Pyrocool Heat Flux Calculation Model

Pyrocool thermal sensor is a water cooled sensor attached to a cooling auxiliary that functions to remove excess heat during a thermal exposure. The model of the heat flow occurring between the copper disk, the sensor housing that contains the copper disk, and the water coolant is illustrated in Figure A1.

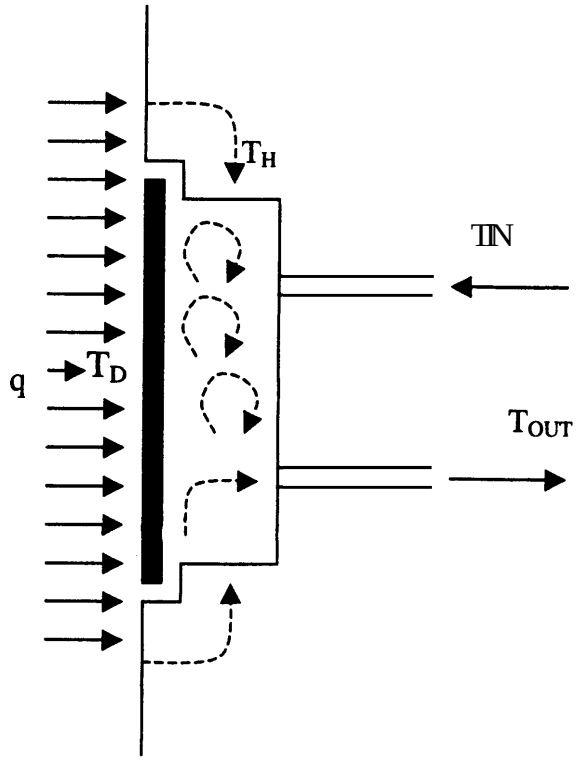

Figure A1. Heat Flow Pattern in the Pyrocool Sensor

Incident heat flux, q, is calculated from the measured temperatures the copper disk, sensor housing , and water coolant using the following thermal balance equation:

$$q = \rho_{CU} C_{P_{CU}} t_{CU} \frac{dT_{CU}}{dt} + h_{CU}(T_D - T_I) - h_H \frac{A_H}{A_{CU}}(T_H - T_I) \qquad \text{(A)}$$

where,

T_I is incoming coolant temperature (C),
T_H is sensor housing temperature (C),
T_{CU} is copper slug temperature (C),
C_{pCU} is copper slug specific heat (kJ/kgC),
ρ_{CU} is copper disk density (kg/m^3),
t_{CU} is copper disk, thickness (m),
A_{CU} is copper disk area (m^2),
A_H is housing wetted area (m^2),
and
h_H and h_{CU} are housing and copper disk heat transfer coefficients (kJ/sec m^2C).

The thermal energy stored by the copper disk, q_{cv}, is:

$$q_{CU} = \rho_{CU} C_{PCU} t_{CU} A_D \frac{dT_{CU}}{dt} \qquad [B]$$

The thermal energy, q_{H2O}, evacuated by the water coolant is:

$$q_{H20} = \dot{m}_{H2O} C_{PH20}(T_0 - T_I) \qquad [C]$$

where

T_0 is the outlet coolant temperature ©,
C_{pH2O} is the coolant specific heat (kJ/kg*K), and
$\dot{m}_{H2O}$ is the coolant mass flow rate (kg/sec).

The heat losses, L, from the sensor housing to the water coolant is estimated as:

$$L = h_H A_H (T_H - T_I) \qquad [D]$$

The transfer of thermal energy from the sensor housing is accounted for by calculating heat transfer coefficients. Therefore, the heat transferred into the water coolant, h_H, is

$$h_H = \frac{A_{CU}}{A_H} * \frac{1}{(T_H - T_A)} \left[\left(\frac{\rho_{CU} * C_{PCU} * t_{CU} * dT_{CU}}{dt} \right) + \left(h_{CU} (T_{CU} - T_A) \right) - q \right] \qquad [E]$$

The heat transfer coefficient for the copper disk, h_{CU}, is

$$h_{CU} = \frac{q_{H2O}}{T_D - T_I} \qquad [F]$$

Figure A2 shows heat transfer coefficients calculated using a constant coolant mass flow rate at three different heat exposures (2.5, 6.3, and 9.66 kW/m^2). Table A1 gives the numerical values of the estimated heat transfer coefficients. Values of the thermal properties and geometrical parameters used in calculating the heat flux are provided in Table A2.

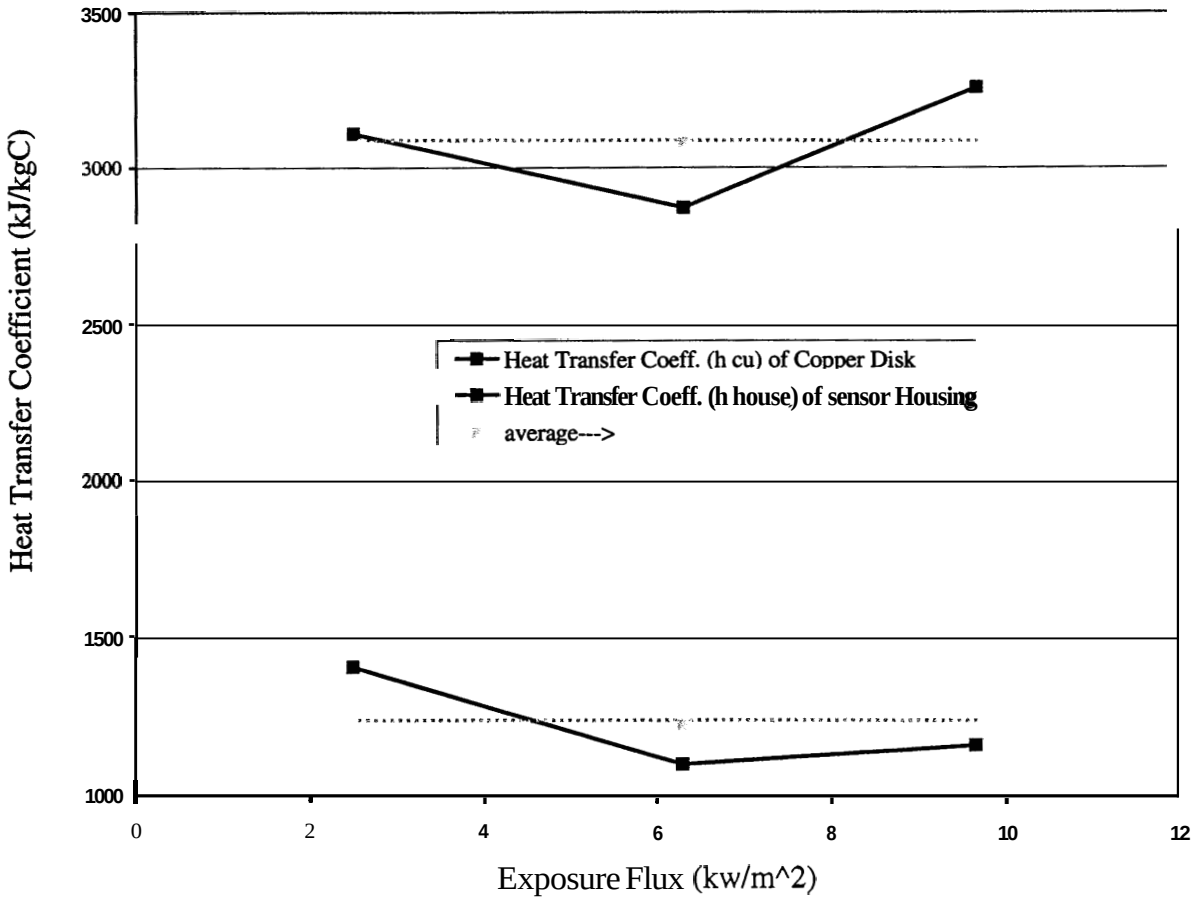

Figure A2. Experimentally Determined Heat Transfer Coefficients of the Copper Disk, h_{CU}, and the Sensor Housing, h_H,

Table A1. Heat transfer coefficients for copper disk h_{CU} and sensor housing h_H.

Exposure (kW/m^2)	h_{CU} ($kJ/sec\ m^2C$)	H_H ($kJ/sec\ m^2C$)
2.5	3111	1406
6.3	2871	1098
9.66	3259	1160
Average	3080	1221

Table A2. Numerical constants used in calculating the heat flux using equation [A] for the Pyrocool sensor

ρ_{CU} (kg/m^3)	C_{PCU} ($j/kg*K$)	t_{CU} (m)	A_{CU} (m^2)	h_{CU} (W/m^2*K)	A_H (m^2)	h_H (W/m^2*K)
8954	381	0.001524	0.00119	3080.62	0.0015	1221.11

Appendix B

Pyrocal Computational Models

Heat Flux Calculations

For a slug calorimeter, heat flux, q, is calculated using the following basic formula:

$$4 = \frac{MCp}{\varepsilon A}\frac{dT}{dt} \quad \text{(A)}$$

where:

q = Incident heat flux (cal/ cm^2·sec),
M = Mass of calorimeter slug (grams),
C, = Heat capacity of copper (cal/g °C),
ε = Surface emissivity,
A = Disk area (cm^2).

For the Pyrocal sensor, a computational method was used to correct for heat losses from the copper disk. For this sensor, heat flux is computed by modifying equation A as:

$$q = \frac{MC_pC_l}{A}\frac{dT}{dt} + K_l(T_d - T_i) \quad \text{(B)}$$

where:

C_l = Thickness factor as experimentally determined,
K_l = Heat loss coefficient as experimentally determined (cal/ cm^2·sec),
T_d = Surface temperature of disk at time t (°C),
T_i = Initial or ambient temperature ("C).

The physical constants used in the heat flux computation sensor are shown in the table below.

Copper Slug Sensor Specifications

Sensor	Mass (g)	Area (cm^2)	ε	C_l	K_l (cal/cm^2·sec· °C)	C, (cal/g °C)
TPP	17.89	12.56	0.95	--	--	0.0927
Insulated copper	1.31	0.99	0.95	1.04	0.00358	0.0927

Additional discussion of this procedure can be found in reference 7.

Bum Injury Prediction

The Stoll criterion was applied to the heat flux read by the Pyrocal sensor to predict time to second degree burn [*8*]. Since the predicted bum times exceed 30 seconds, an exponential decay extrapolation of the Stoll data is used.

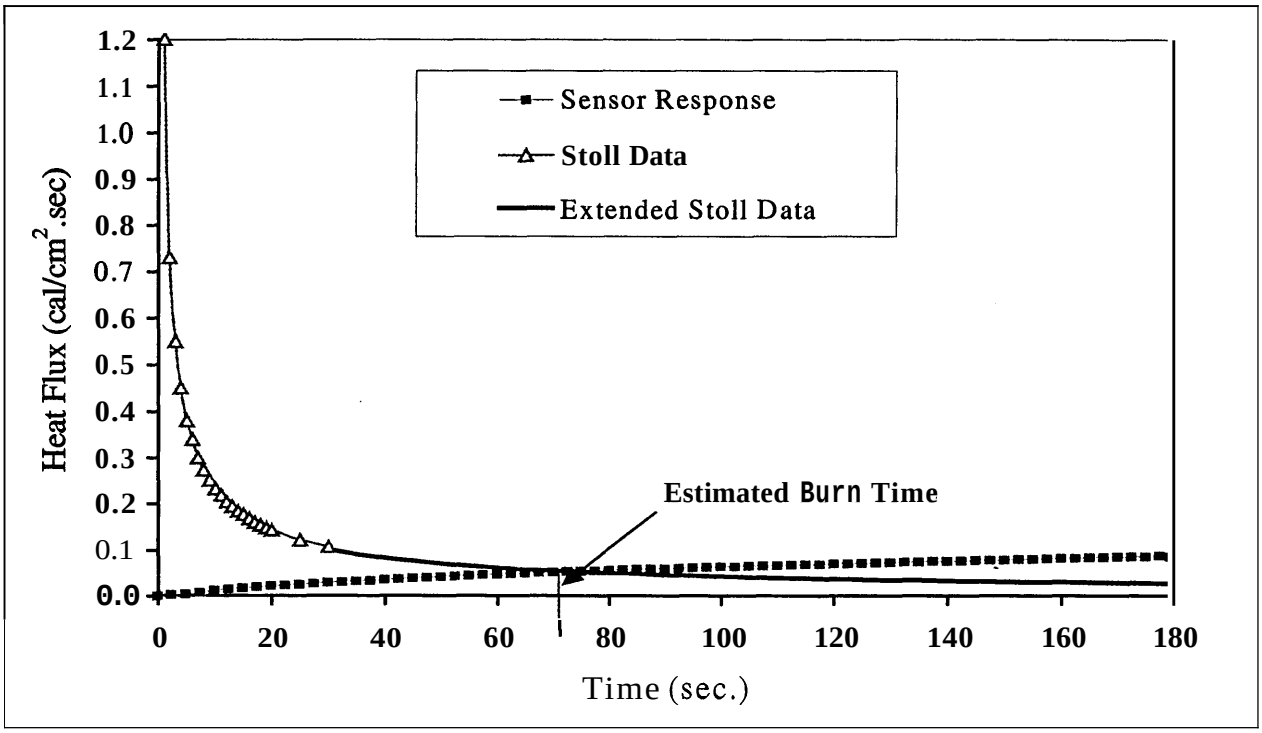

Figure B 1. Estimating Second Degree Bum Using Exponential Extrapolation of Stoll Data.

As estimated in Figure B 1, second degree bum time is estimated by the intersection of the exponentially extrapolated Stoll curve and the data generated by the sensor.

Appendix C

Thesis Draft

A LIQUID COOLED HEAT FLUX TRANSDUCER FOR USE IN EVALUATING THE THERMAL PROTECTIVE PERFORMANCE OF FIREFIGHTER CLOTHING

by

Darren Winfred Heath

TABLE OF CONTENTS

LIST OF FIGURES

LIST OF TABLES

Table Number

ACKNOWLEDGMENTS

The author wishes to express sincere appreciation to Dr. Roger Barker, Dr. Hechmi Hamouda and Dr. James Leach for their assistance in the preparation of this manuscript. A special thanks goes to the late **Mr.** Malcolm Bender for his in-depth knowledge and assistance on this project. I would also like to personally thank **Mr.** Jim Fowler and Shawn Deaton whose familiarity with the needs and ideas of the thermal protection and comfort lab was extremely helpful during the entire phase of this undertaking. Much thanks also to **Mr.** Robert V. Grimes, Dr. Itzhak Shalev, **Mrs.** Gail Liston, and Cordula Guerth for their invaluable assistance on the project. Also, a warm and loving thanks goes out to my tremendously supportive family Troy, Debbie, Melissa, Laura and my beautiful wife Elizabeth.

Finally, the author would like to thank the National Institute of Standards and Technology as well as North Carolina State College of Textiles for their financial support for this project.

Chapter 1

FIREFIGHTER THERMAL EXPOSURE

In order to select appropriate test methods and thermal sensor specifications, the conditions under which protective clothing will be used must be considered. However, it is quite difficult to completely define the firefighter environment. This is due to the many environmental, physical, physiological and psychological factors that effect a firefighter's interaction with the fire scene. Nonetheless, data has been collected and information is available to provide a range of common thermal environment conditions that are classified into three general categories. These classifications are identified as Routine, Hazardous and Critical, and are described in detail below.

Routine Conditions: These conditions are applicable to firefighters who are operating hoses or otherwise fighting fires from a distance, where no special clothing is necessary. According to Foster et al. [6], the limits proposed are 25 minutes at 100 °C and a thermal radiation limit of $1 kW/m^2$ ($0.024 cal/cm^2 sec$). According to Abbott et al. [13], routine conditions are those experienced in front of a small open fireplace, and present no real hazard to the firefighter. The firefighter can remain close to the fire safely without any protective clothing for a minute or two and extinguish it. Abbott associates conditional limits of 20-70 °C with thermal radiation of $< 1.7 kW/m^2$ ($0.04 cal/cm^2 sec$).

Hazardous Condition: These conditions (described as "Ordinary" by Abbott et al.) [1], are typical of those that would be encountered outside a burning room or small burning building. As reported by Hoschke [7], the lower bounds of this region are similar to firefighters ventilating a fire without water support, while the upper limits are applicable to those who are first into a burning building. Nonetheless, a "turnout" uniform is necessary to provide burn protection and to minimize thermal stress the firefighter may encounter. The range set by Foster et al. [6] has been taken to be at least 1 minute at 160 °C and a thermal radiation of $4 kW/m^2$ ($0.096 cal/cm^2 \cdot sec$) and can be tolerated up to 10 minutes. Abbott et al. [1] describe this condition as lasting 10-20 minutes with air temperatures of 70 "C-300°C with thermal radiation of $0.4 kW/m^2$ to $12.6 kW/m^2$ ($0.04 cal/cm^2 \cdot sec$ to $0.30 cal/cm^2 \cdot sec$). Recent work has shown that some simple wastebasket fires may output up to $40 kW/m^2$.

Critical Condition: These conditions (described as "Emergency" by Abbott et al.) [1], are not normally encountered by civilian firefighters. These conditions exist around a crashed aircraft when fiercely burning fuel exists. They m y also be encountered during "flashover" of a large building fire. A proximity suit as well as special breathing apparatus must be employed when working with fires in this condition [8]. These conditions as described have been taken to be above the range of "Hazardous" conditions and reaching beyond 235 °C in temperature

and 10 kW/m^2 in heat flux (0.23 cal/cm^2sec) by Foster et **al.** [6]. Severe thermal problems and life threatening injuries are associated with these conditions. Abbott et **al.** [1] describe these conditions as having temperatures ranging from 300 "C to 1200 "C and heat flux between 12.6 kW/m^2 and 209 kW/m^2 (0.30 cal/cm^2sec to 5.0 cal/cm^2sec).

MEASUREMENTS IN PROLONGED THERMAL EXPOSURES

Application conditions, therefore, clearly indicate a need to evaluate the protective performance of firefighter clothing materials using conditions that simulate thermal exposures occurring near, or outside a flash fire environment. These firefighting conditions typically involve exposures to radiant thermal energy for periods that may last for several minutes. These conditions can exceed the useful range of calorimeter or slug type sensors, which are limited to relatively short exposure durations. The use of thermocouples presents a separate set of technical challenges including the ambiguities involved in heat flux calculation and skin burn injury estimation from thermocouple readings.

This research involved the development and design of a dynamically cooled thermal flux sensor that can be used to measure the thermal protective performance of firefighters clothing in prolonged exposures to heat. The main objective of this effort was to demonstrate the conceptual feasibility and evaluate the prototype as a useful instrumental approach for this ranging of applications.

Chapter 2

WATER COOLED PROTOTYPE SENSOR

The thermal sensing system consisted of a water-cooled sensor, heat sensing thermocouples, and cooling auxiliaries (Figure 2.1). The sensor assessed incident heat flux by measuring the temperature of the sensor and water flowing through the system.

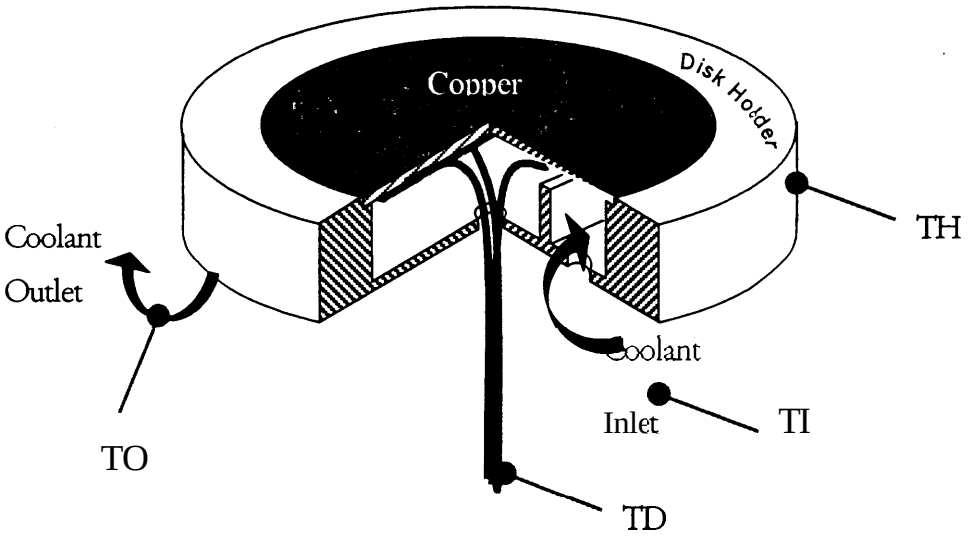

Figure 2.1: NCSU Water Cooled Prototype System

A mathematical method was developed to calculate heat flux using temperature readings, heat transfer coefficients and the physical properties of the system

Mathematical *Model*

The following formula was used to calculate the heat flux read by the prototype sensor:

(Total Heat** Flux)* = ***(Energy Stored in Copper Disk) + ***(Energy Stored in Water)*** − ***(Energy Stored in* Housing)**

or,

$$q = \rho_{CU} C_{P_{CU}} t_{CU} A_{CU} \frac{dT_{CU}}{dt} + \dot{m}_{H20} C_{P_{H20}} (T_I - T_O) - h_H A_H (T_H - T_I) \qquad [A]$$

where,

T, is the incoming coolant temperature (K)

T_O is the exit coolant temperature (K)

T_{CU} is the temperature of the copper slug

T_H is the sensor housing temperature (K)

ρ_{CU} is the density of the copper disk (kg/m^3)

C_{pCU} is the specific heat of the copper slug (kJ/kg*K)

t_{CU} is the thickness of the copper slug (m)

A_{CU} is the area of the copper disk (m^2)

t is the time step of the experiment (sec)

$\dot{m}_{H20}$ is the mass flow rate of the coolant (kg/sec)

C_{pH20} is the specific heat of the coolant (kJ/kg*K)

h_H is the heat transfer coefficient of the sensor housing ($kJ/sec*m^2*K$)

A_H is the wetted area of the sensor housing (m^2)

The thermal energy measured by the copper disk q_{CU} is calculated as

$$\rho_{CU} * C_{PCU} * t_{CU} * A_D * \frac{dT_{CU}}{dt} = q_{CU} . \qquad [B]$$

The thermal energy absorbed by the water cooling the system, q_{H2O}, is

$$\dot{m}_{H2O} * C_{PH2O} * dT_{H2O} = q_{H2O} . \qquad [C]$$

The thermal energy transfer from the sensor housing into the water coolant is estimated as follows:

$$h_H * A_H * (T_H - T_I) = L \qquad [D]$$

where L is the energy stored in the sensor housing, or the heat losses from the system.

The transfer of energy from the sensor housing is accounted for by calculating heat transfer coefficients. Therefore, the heat transferred into the water coolant, h_H is estimated as

$$\frac{A_{CU}}{A_H} * \frac{1}{(T_H - T_A)}\left[\left(\frac{\rho_{CU} * C_{PCU} * t_{CU} * dT_{CU}}{dt}\right) + \left(h_{CU}(T_{CU} - T_A)\right) - q\right] = h_H . \qquad [E]$$

The heat transfer coefficient for the copper disk, h_{CU} is

$$q_{H2O} \Big/ (T_D - T_A) = h_{CU} . \qquad [F]$$

By manipulating the above equations, heat transfer in the sensor is estimated as:

$$q = \rho_{CU} C_{P_{CU}} t_{CU} \frac{dT_{CU}}{dt} + h_{CU}(T_D - T_I) - h_H \frac{A_H}{A_{CU}}(T_H - T_I) . \qquad [G]$$

This equation is used extensively throughout the remainder of the report. Figure **2.2** show the results of the calculating the heat transfer coefficients using a constant coolant **mass** flow rate and three different heat exposure conditions of 2.5, 6.3, and 9.66 kW/m^2. Table **2.1** gives the numerical values of the heat transfer coefficients for thermal exposures of 2.5, 6.3, and 9.66 kW/m^2, using a

constant coolant flow rate. Values of the thermal properties and geometrical parameters used in calculating the heat flux are given in Table 2.2.

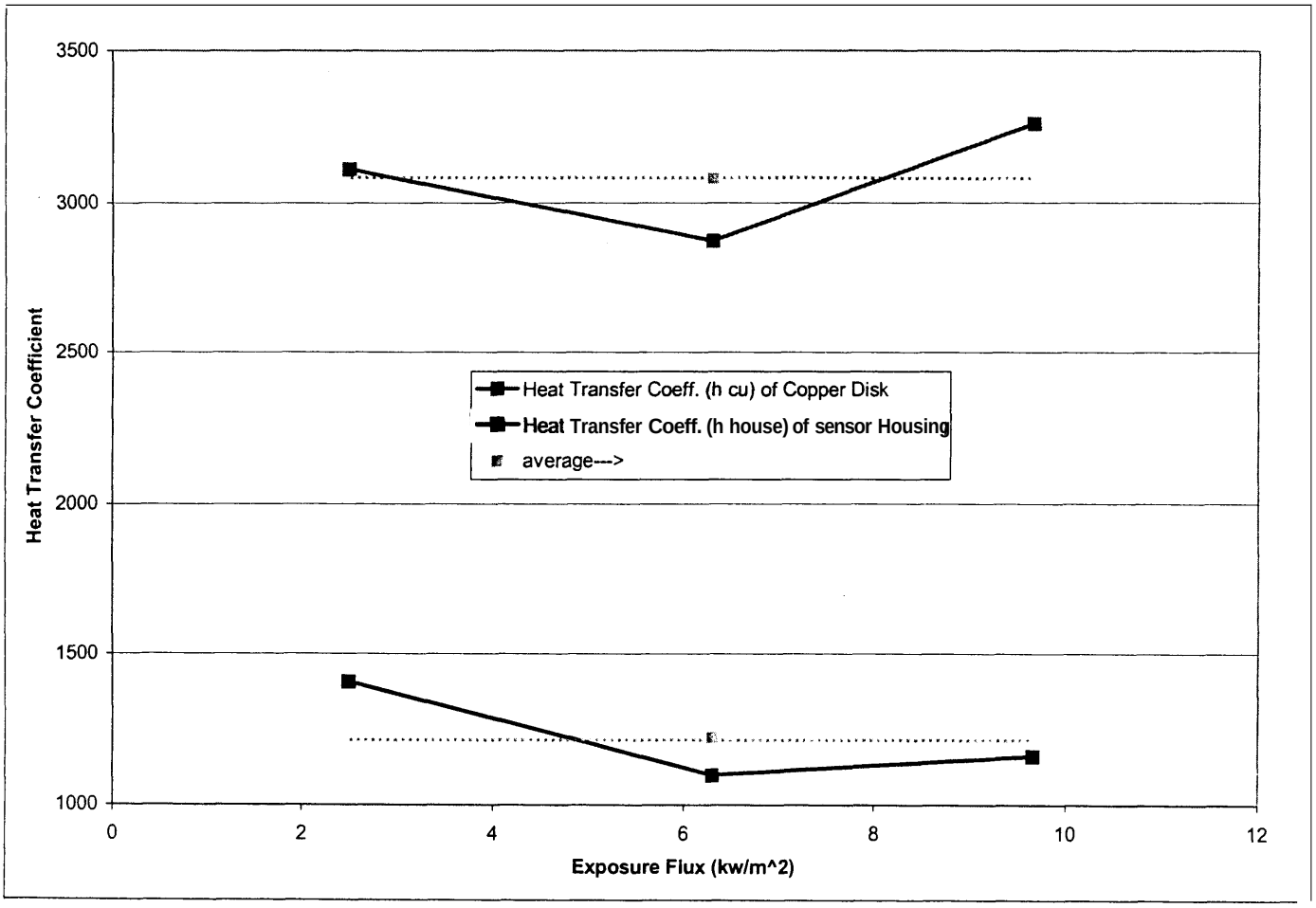

Figure 2.2: Experimentally determined heat transfer coefficients of the copper disk, h_{CU}, and the sensor housing, h_H,

Table 2.1: Heat transfer coefficients for the copper disk h_{CU} and of the sensor housing h_H.

kW/m^2	Heat Transfer Coefficient of Copper Disk h_{CU}	Heat Transfer Coefficient of Sensor Housing h_H
2.5	3111	1406
6.3	2871	1098
9.66	3259	1160
Average		
Average	3080	1221

Table 2.2: Numerical constants used in calculating the heat flux using equation [G] of the liquid cooled prototype sensor

cu (kg/m^3)	C_{PCU} (j/kg*K)	t_{CU} (m)	A_{CU} (m^2)	h_{CU} ($W/m^{2*}K$)	A_H (m^2)	h_H ($W/m^{2*}K$)
8954	381	.001524	0.00119	3080.62	0.0015	1221.11

Chapter 3

DESCRIPTION OF SENSORS USED FOR THE COMPARISON STUDY

This research identified five sensors including the NCSU water cooled prototype sensor, the Thermogauge™ [9], Hy-Therm@[10], NCSU Pyro-Cal, Thermoman® or skin simulant, and the standard TPP sensor for comparison testing. In addition to the above sensors, a t-type thermocouple was used in the study.

Thermogauge™

This sensor is a circular foil heat flux gauge that operates by measuring the temperature differential between the center and the circumference of a thin constantan foil disk. The constantan foil disk is bonded to a cylindrical copper heat sink. The incident heat is drawn towards the heat sink away from the center of the constantan foil. This produces a temperature drop across the constantan foil, which is measured by the thermoelectric junctions in the center of the constantan foil and the outer copper heat sink. The voltage output from the sensor is read and combined with a calibration coefficient, provided by the manufacture, to calculate the absorbed heat flux.

Hy-Therm®

The Hy-Therm® sensor consists of an insulating wafer with a series of thermocouples embedded in the backside of the wafer in such a way that the thermoelectric junctions fall on opposite sides of the insulating wafer. The wafer is mounted to a heat sink that draws the incident heat. A temperature drop will result across the wafer and the thermocouples respond to this drop. The thermocouples are connected in series, which provides an additive or amplified response in the output. The output is then proportional to the heat flux incident upon the sensor.

TPP

The TPP sensor or Thermal Protective Performance sensor is an insulated copper slug calorimeter. This sensor is not cooled and has been proven in the industry as a rugged and reliable sensing device that is well established for heat flux measurements and the prediction of human tissue damage.

NCSU Pyro-Cal

The NCSU Pyro-Cal sensor was developed at the Center for Research on Textile Protection and Comfort (T-PACC) at NCSU for use in the PyroMan flame test manikin. The NCSU Pyro-Cal sensor consists of a thin copper disk surrounded by a radial thin copper ring acting as a thermal guard. Both the copper disk and

the copper ring are held in place by an insulating holder to minimize heat transfer to and from the body of the calorimeter thus approximating one-dimensional heat flow. A T-type (copper-constantan) thermocouple is attached to the backside of the copper disk. The whole assembly is encased within a metallic and ceramic protective shell [11].

Thermoman ®

The Thermoman ® sensor or Embedded Thermocouple Sensor, is the sensor that is currently in operation in the full-scale mannequin NCSU Pyro-Man flame retardant garment test. It is a thin-skin calorimeter which utilizes a Type T thermocouple. The thermocouple is buried below the exposed surface of the cast thermoset polymer resin plug at a depth of 0.127 mm (0.005 in). The polymer reportedly exhibits a thermal inertia, $(k\rho C_p)$, similar to that of undamaged human skin [11]. The Embedded Thermocouple Sensor is designed with a frontal thickness greater than 6.35 mm (0.25 inch) such that temperature conditions along the rear side of the sensor will not affect the response of the surface measurements. This allows the sensor to be considered an infinite thickness slab, utilizing the infinite slab geometry for the exposure. Noting that the depth of the thermocouple is critical to the analysis of the heat flux in this sensor, a computer program is used to calculate heat flux.[11] The methods used to calculate heat flux for each of these sensors is described in Appendix E.

Chapter 4

EXPERIMENTAL

RADIANT PROTECTIVE PERFORMANCE PANEL

In conducting a comparative *study* of the performance of different sensors, the RPP test platform **was** used [12]. An exploded view of the RPP testing stand can be seen in figure 4.1. **A** photograph of the RPP testing stand can be seen in Figure 4.2. The RPP contains a mounting assembly that is 5 inches by 5 inches **by** 2 inches high, (Figure **4.3).** It uses quartz radiant heater tubes to provide a stable heat source.

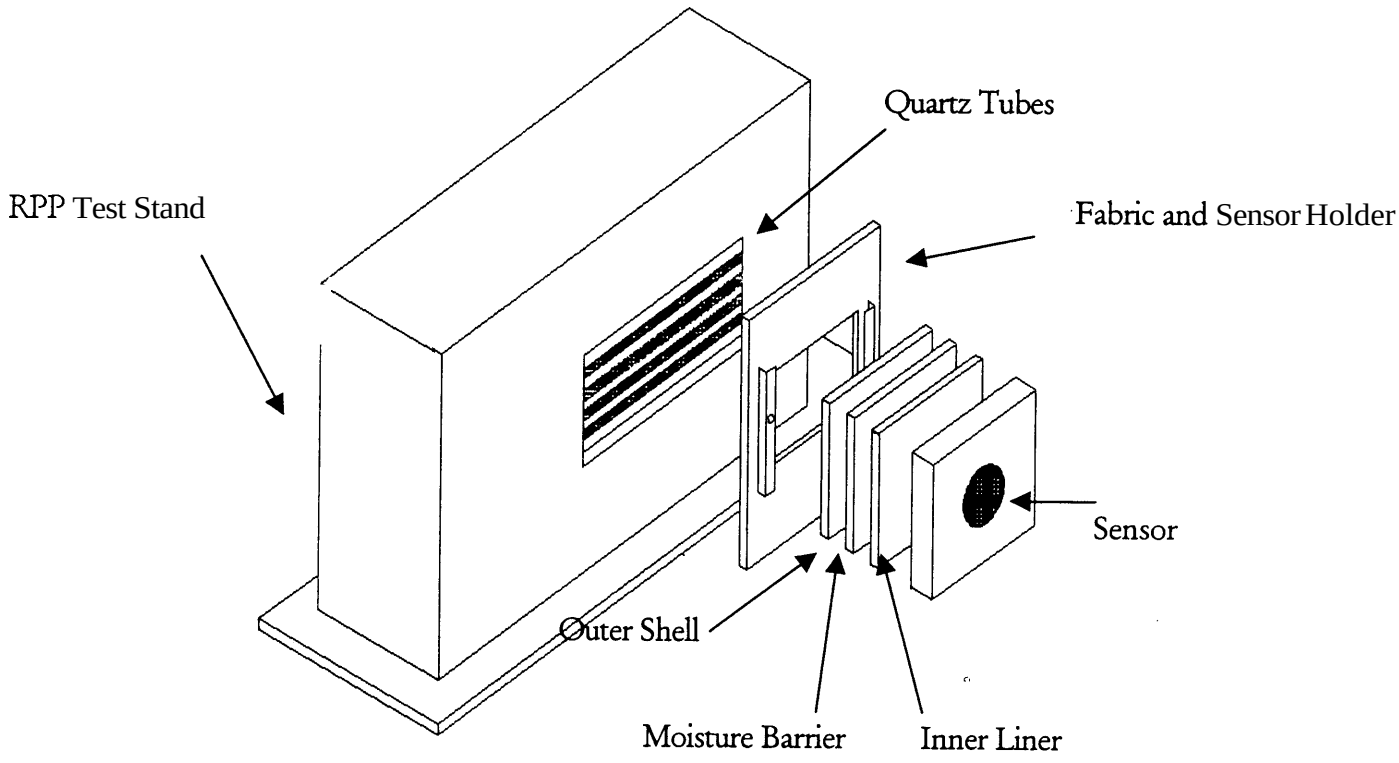

Figure 4.1: Exploded view of RPP Testing Stand

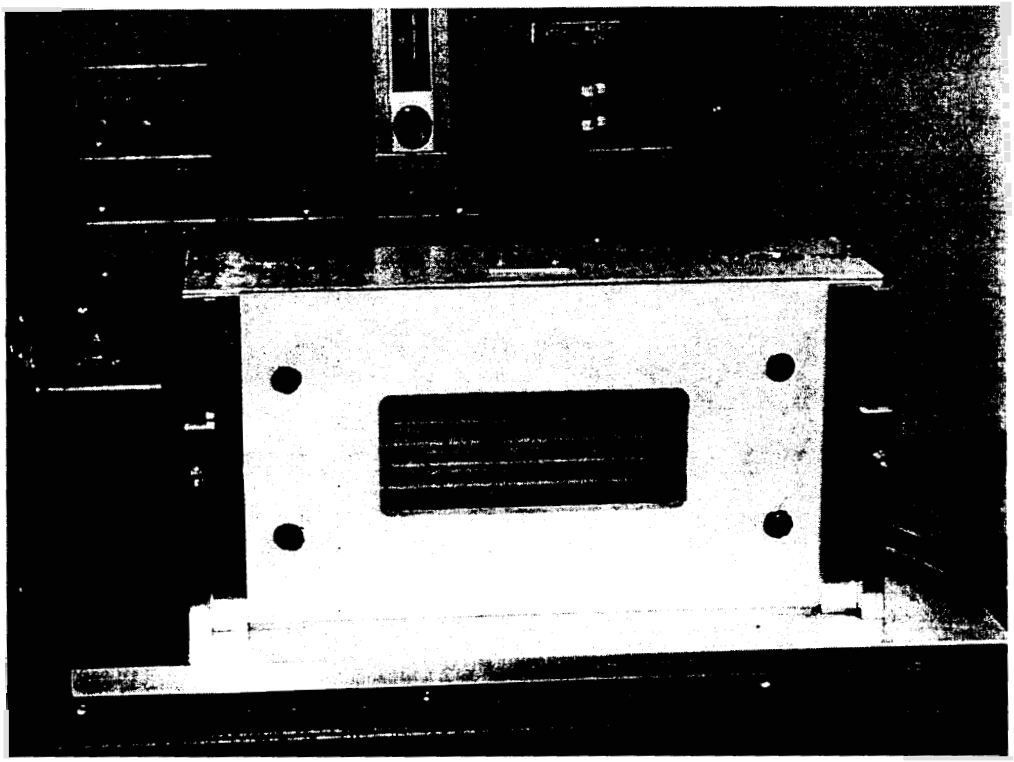

Figure **4.2:** Photograph of RPP Testing **Stand**

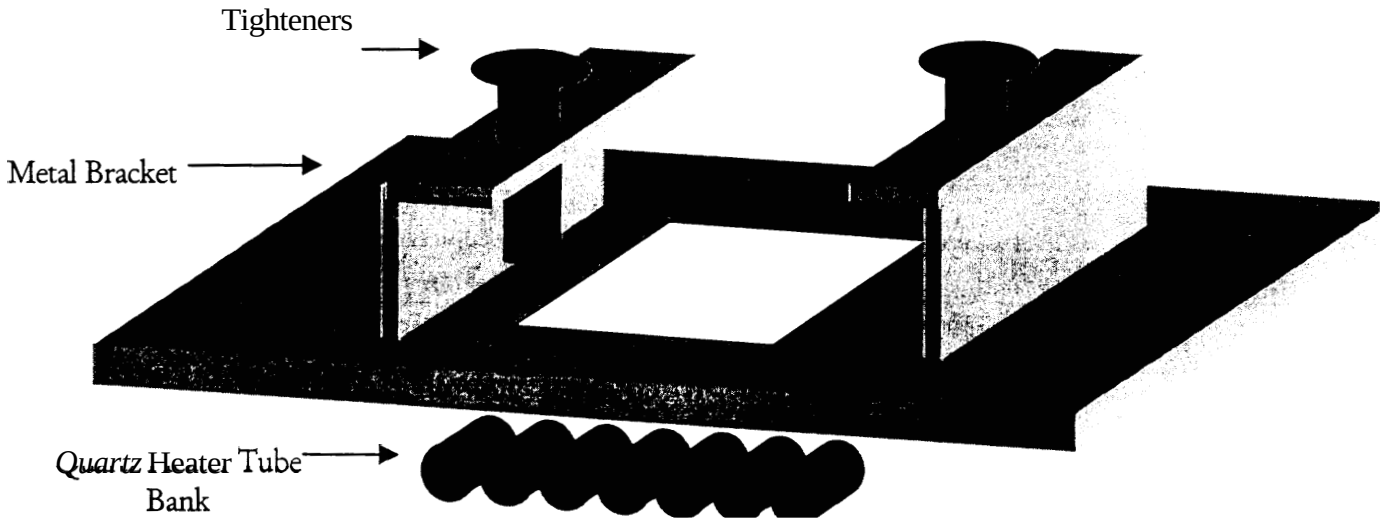

Figure **4.3:** Metal bracket used to hold sensors during testing.

COMPARATIVE STUDIES

Direct Sensor Response

Direct Sensor Exposure

A two-part comparison study using the RPP assembly was conducted. The first part of the study compared sensor response in direct exposures to the heat source. The aim of this series of experiments was to evaluate the response of each type of sensor without a fabric or test garment in place. The TPP sensor was used to establish the intensity of the thermal exposure.

Figures 4.4, 4.5, and 4.6, show the response of the test sensors at 2.5, 6.3, and 9.6 kw/m^2, (0.06, 0.15, 0.23 cal/cm^2*sec), for a 5-minute exposure. The heat flux read by the TPP sensor is observed to drop off during the lengthy exposure. This phenomenon is also observed in the response of the Thermoman®, although the drop off is not as pronounced as with the TPP. Both the calorimeter type and the embedded thermocouple type sensor are constructed of materials that retain thermal energy during the exposure sequence. Consequently, the internal temperature of this type of sensor rises to levels that make the sensor unable to accurately differentiate incident heat flux. The heat flux indicated by the Pyro-Cal sensor is observed to trail up during the exposure. This is due to computational methods used to compensate for the heat storage effects from the

copper disk REFERENCE. These experiments demonstrate that only the liquid cooled sensors, Hy-Therm? Thermogauge™ and the NCSU Water Cooled Prototype, provide a stable reading of incident heat flux throughout the five minute duration of the thermal exposure. The liquid cooled sensors are able to dissipate the stored thermal energy, which tends to saturate non-cooled slug-type sensors. In addition, the liquid cooled sensors provide the closest response to the set thermal exposure.

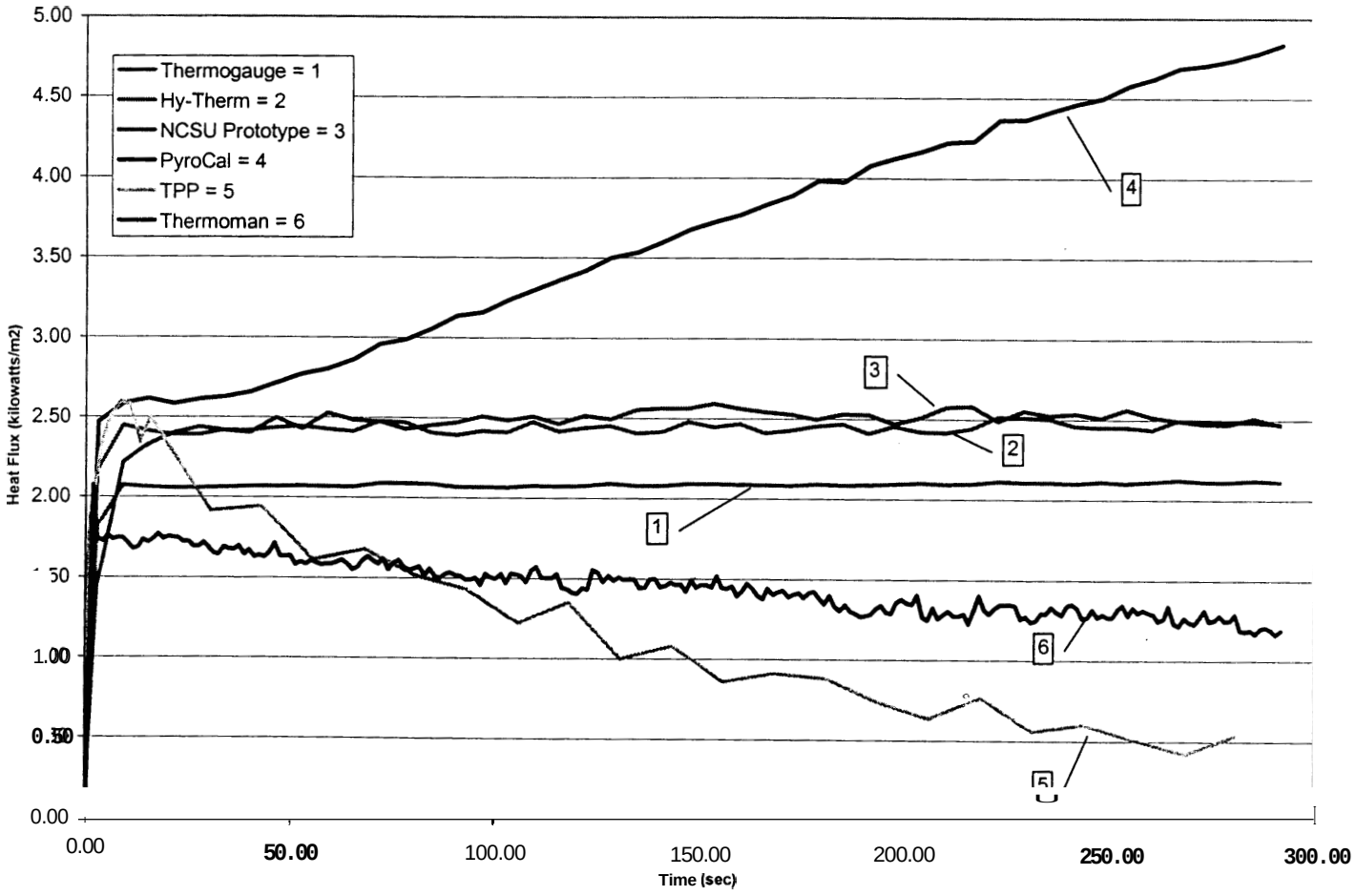

Figure **4.4:** Direct sensor exposure at **2.5** kilowatts/m^2 (0.06 cal/cm^{2}*sec).

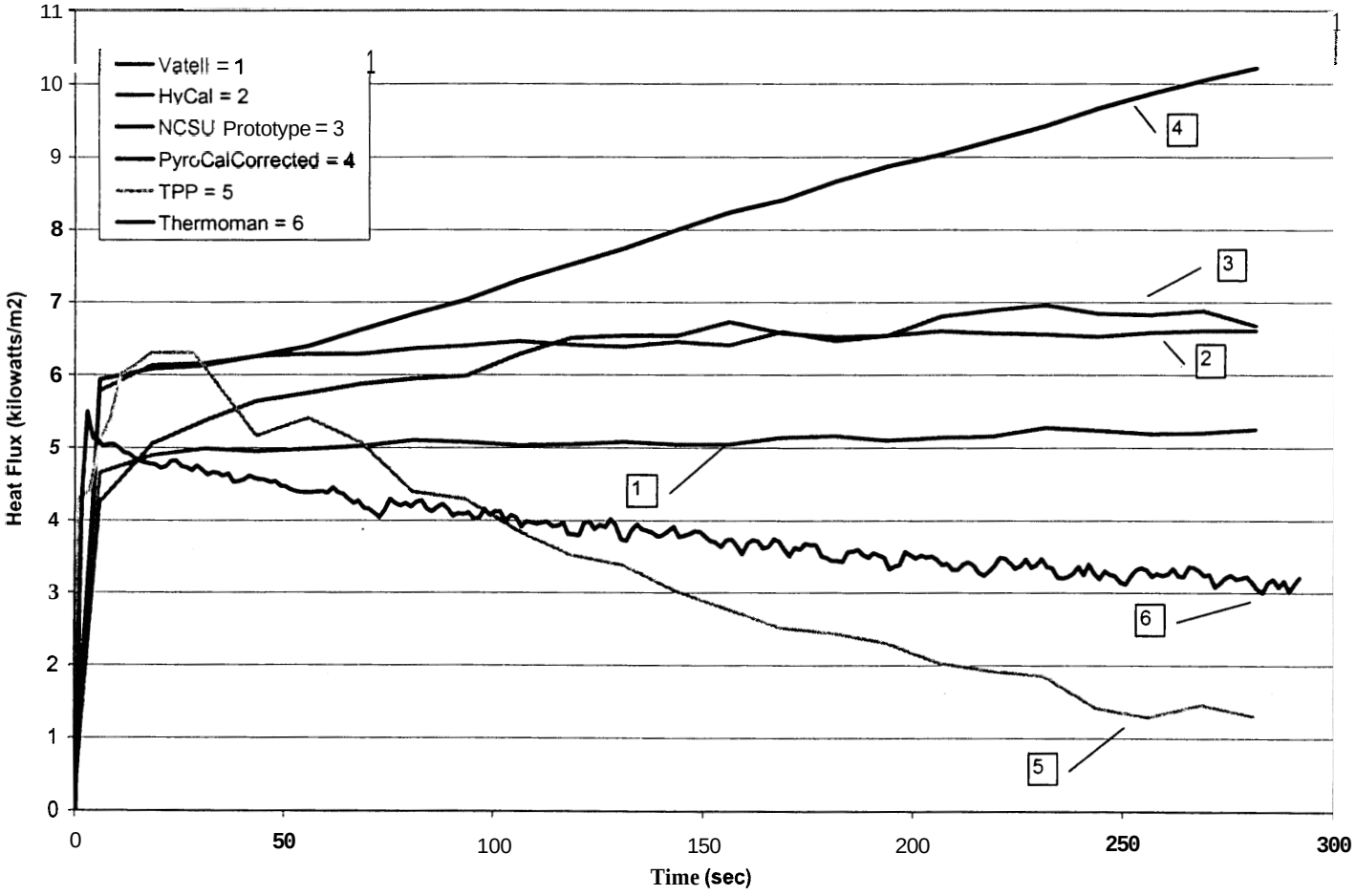

Figure 4.5: Direct sensor exposure at 6.3 kilowatts/m^2 (0.15 cal/cm^{2}*sec).

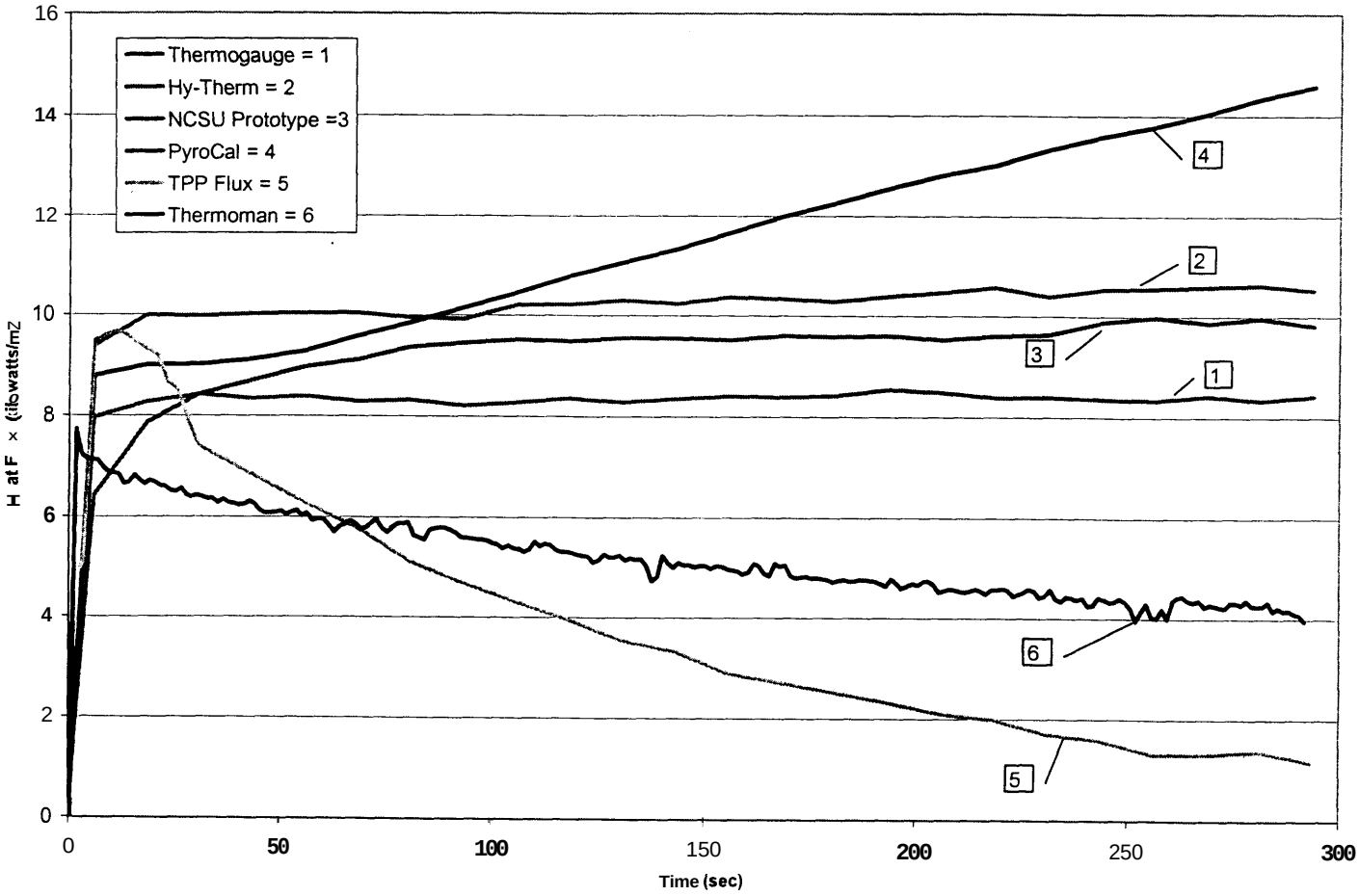

Figure **4.6:** Direct sensor exposure at 9.6 kilowatts/m^2 (0.23 cal/cm^{2}*sec).

RPP Response

RPP Experiments

The second part of the *study* compared sensor readings of heat transfer through firefighter turnout materials. The goal of these experiments was to compare the response of each sensor in recording heat transfer, and in predicting time for skin damage to occur when placed behind firefighter turnout material.

A firefighter turnout composite, consisting of a 6.00 oz/yd² Kevlar® / PBI shell fabric, crosstech on E89 moisture barrier and Arawool® thermal liner was exposed to three different levels of heat exposure: 2.5, 6.3, and 9.66 kw/m², (0.06, 0.15, 0.23 cal/cm²*sec). Heat transfer was then measured, at each of these exposures, using each of the sensor types of interest, including the Pyro-Cal®, Thermoman®, Thermoguage™ , TPP, and the NCSU Water Cooled Prototype. An additional experiment was performed using a T-type thermocouple sewn to the facecloth side of the thermal liner component to indicate temperature readings for these thermal exposures. Figure 4.7.

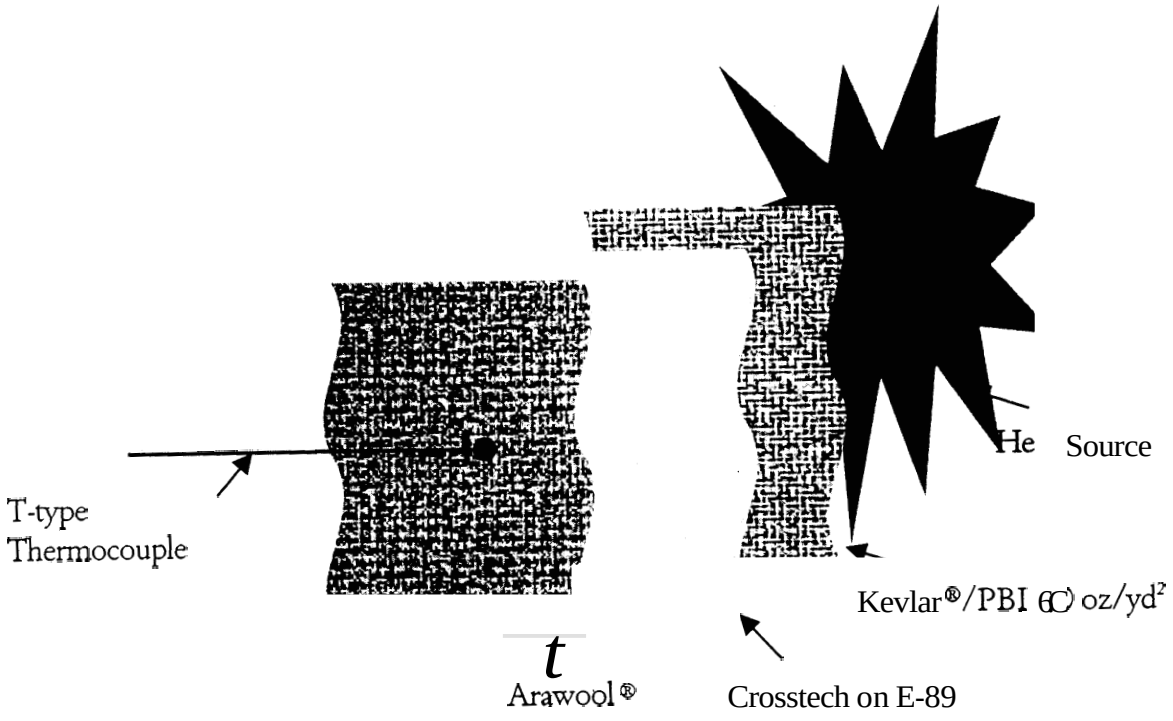

Figure 4.7: T-type thermocouple sewn to the backside of firefighter turnout material.

Figures 4.8, 4.9, and 4.10 show the response of the selection of the test sensors during RPP exposures of 2.5, 6.3, and 9.6 kw/m². The Hy-Therm@was not operated behind test garments for fear of damaging the sensor beyond repair due to the degradation of the fabric. It should be noted that the the Thermoman® sensor requires a calibration coefficient in order to be operated accurately when used in the Pyro-Man® manikin at the College of Textiles at N.C. State. This calibration coefficient is based on the intensity of the heat source used for

calibration. The calibration coefficient can and does change as the incident heat flux changes. Due to this phenomenon, during the RPP exposures, the Thermoman® sensor was used "as is" meaning no calibration coefficient was used. The results of all the test discussed are based on the average of triplicate measurements.

Several important factors can be inferred from figures **4.8,** 4.9, and 4.10. The Thermogauge™ and the NCSU Water Cooled Prototype provided a realistic response to the dynamic transfer of heat energy through the fabrics. These two sensors do reach a steady state and continue to operate reliably throughout the remainder of the exposure sequence. The Pyro-Cal sensor provided somewhat of a realistic response to the dynamic heat transfer through the test fabric due to how the losses factor behaves within its heat flux calculation equation. As was seen in the direct exposure sequences, the Pyro-Cal sensor trailed up in its response. Observing that the losses factor is temperature dependent, and the sensor disk temperature does not approach critical levels, the losses factor does not overpower the equation and the response remains stable. During the RPP exposure of lower incident heat fluxes, the fabric is protecting the Pyro-Cal sensor from becoming saturated with heat and enables the sensor to respond for an extended period of time verses what was observed in the direct exposure sequence. The TPP sensor behaves in much the same as did in the direct sensor exposure. The TPP sensor becomes saturated with heat and the response trailed

off during the exposure sequence. This same trend can also be observed in the response of the Thermoman® sensor. The non-cooled polymer sensor becomes saturated with heat which causes the sensor to be unable to distinguish internal temperatures from surface temperatures.

Figure 4.11 provides the response of the T-type thermocouple that was sewn onto the back of the test garment during the RPP exposure. Each of the three thermocouples provides the same basic trend in the 300-second exposure at the three different levels of incident heat flux.

Table 4.1 shows the second-degree burn estimates made using different types of thermal sensors. The Stoll criterion was used to predict time to second degree bum for the TPP, Pyrocal, and the water-cooled sensor [13,14]. The skin model burn translation algorithm was used in the Thermoman® sensor. This bum model is based on criteria suggested by Henriques [15]. Bum predictions obtained from these sensors compared with an estimate based on the temperature registered by a thermocouple attached to the innermost thermal liner fabric of the turnout composite. In this case, a criterion used in recent work by NIST and 3M was applied: the innermost fabric surface temperature of 55 C is used as an indication of the potential for second-degree bum [16]. According to Neal, the amount of protection time fabric yields prior to achieving a second

degree burn are higher when using a skin burn model approach verses using the surface temperature of the innermost fabric layer.[17]

Table 4.2 provides values of the times each sensor, including the thermocouple, took to register an absolute delta, or rise in temperature, of 25°C and of 55°C. This allows for various interpretations of the response of the sensor to be concluded.

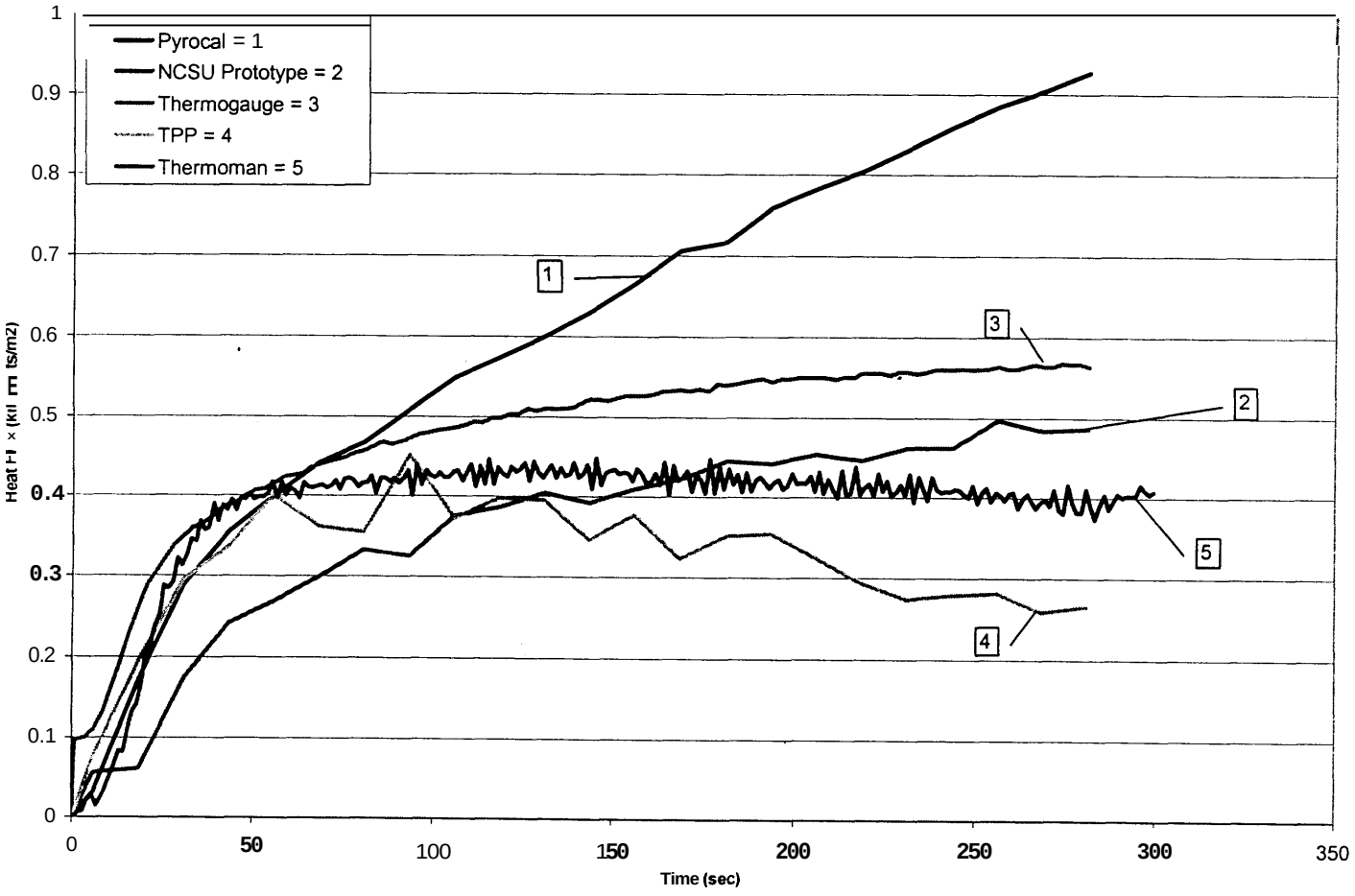

Figure 4.8: RPP **exposure** at 2.5 kilowatts/m^2 (0.06 cal/cm^{2}*sec)

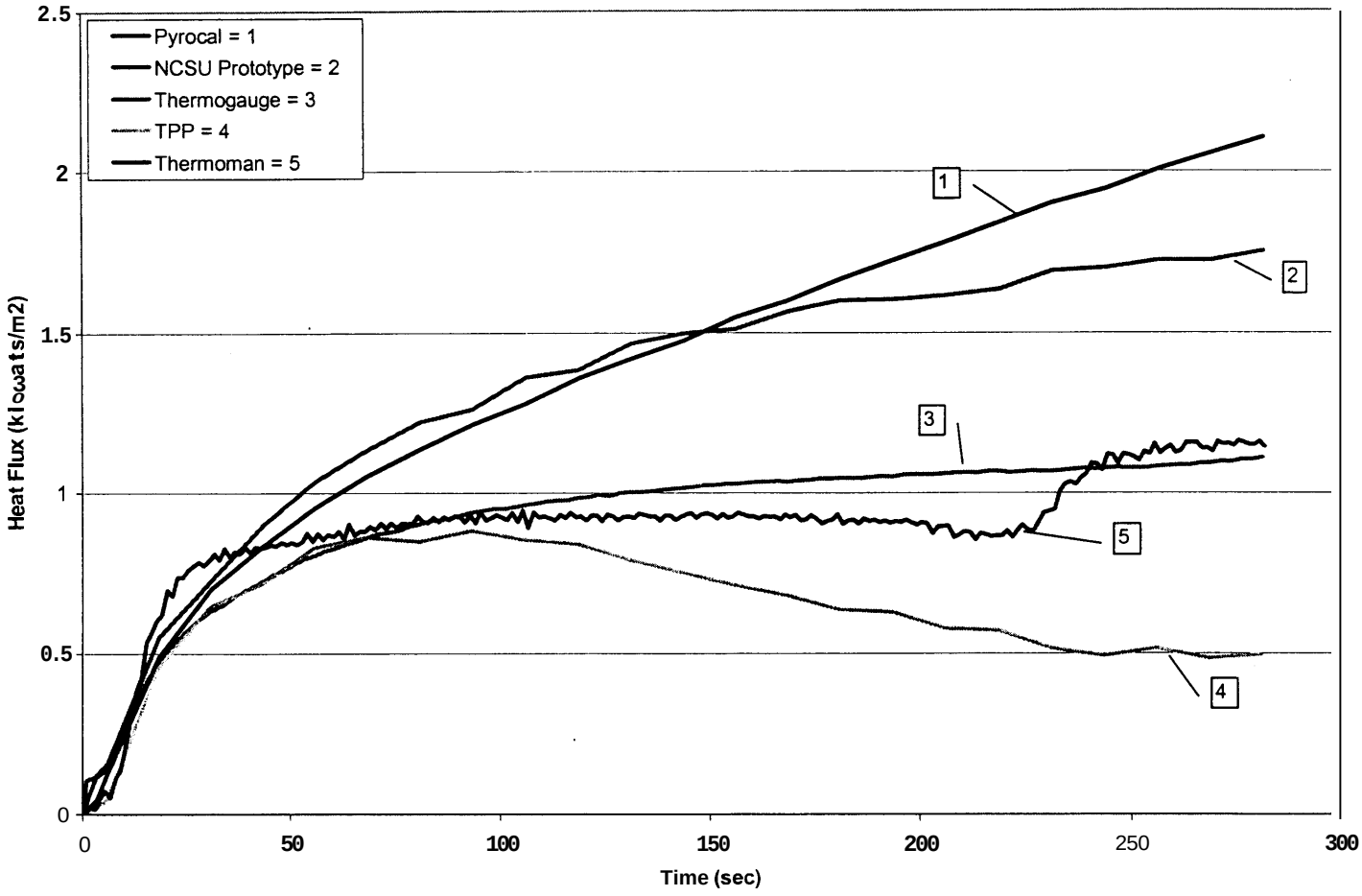

Figure **4.9:** RPP exposure at 6.3 kilowatts/m^2 (0.15 cal/cm^{2}*sec)

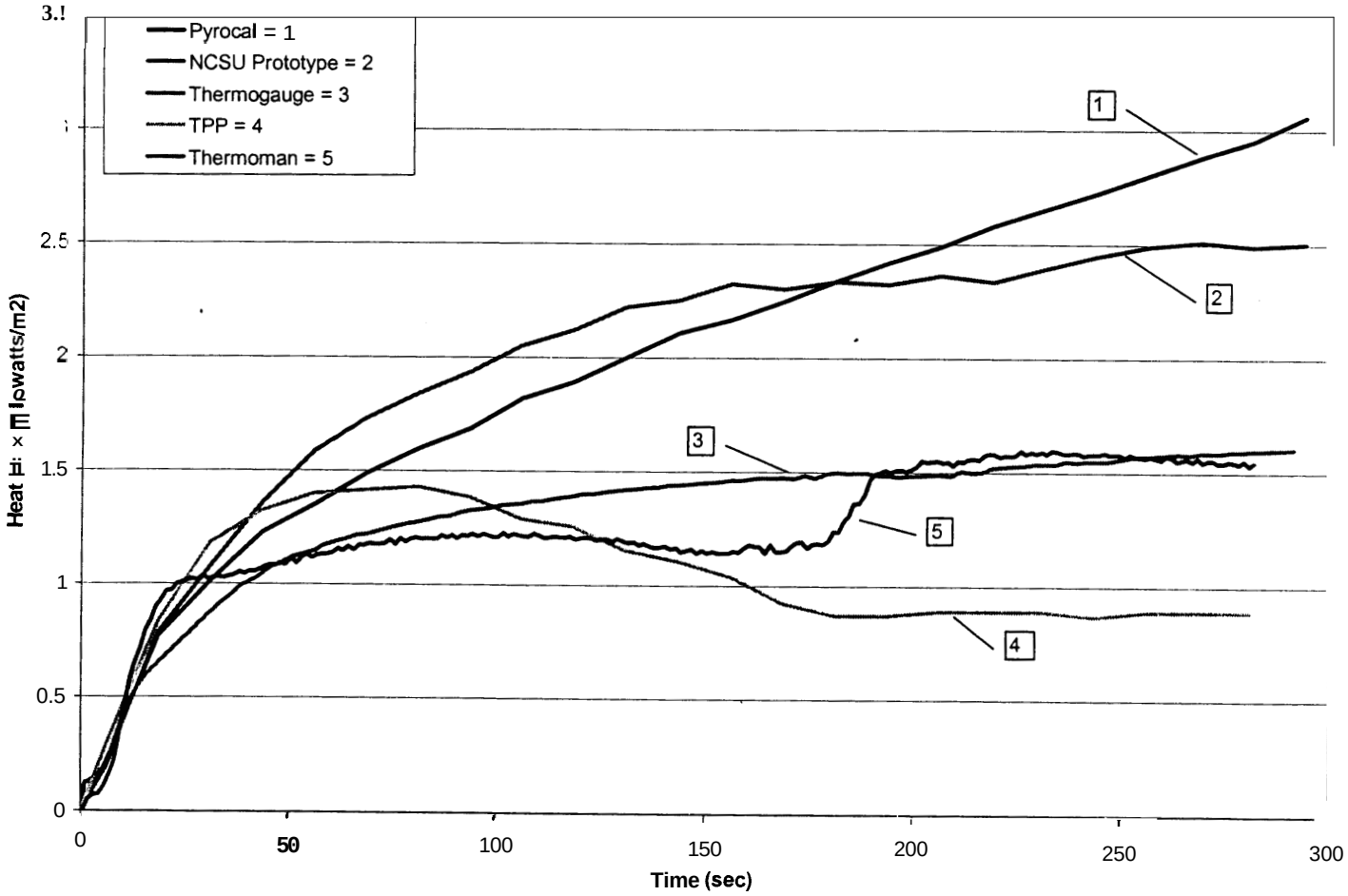

Figure 4.10: RPP exposure at 9.66 kilowatts/m^2 (0.23 cal/cm^{2}*sec)

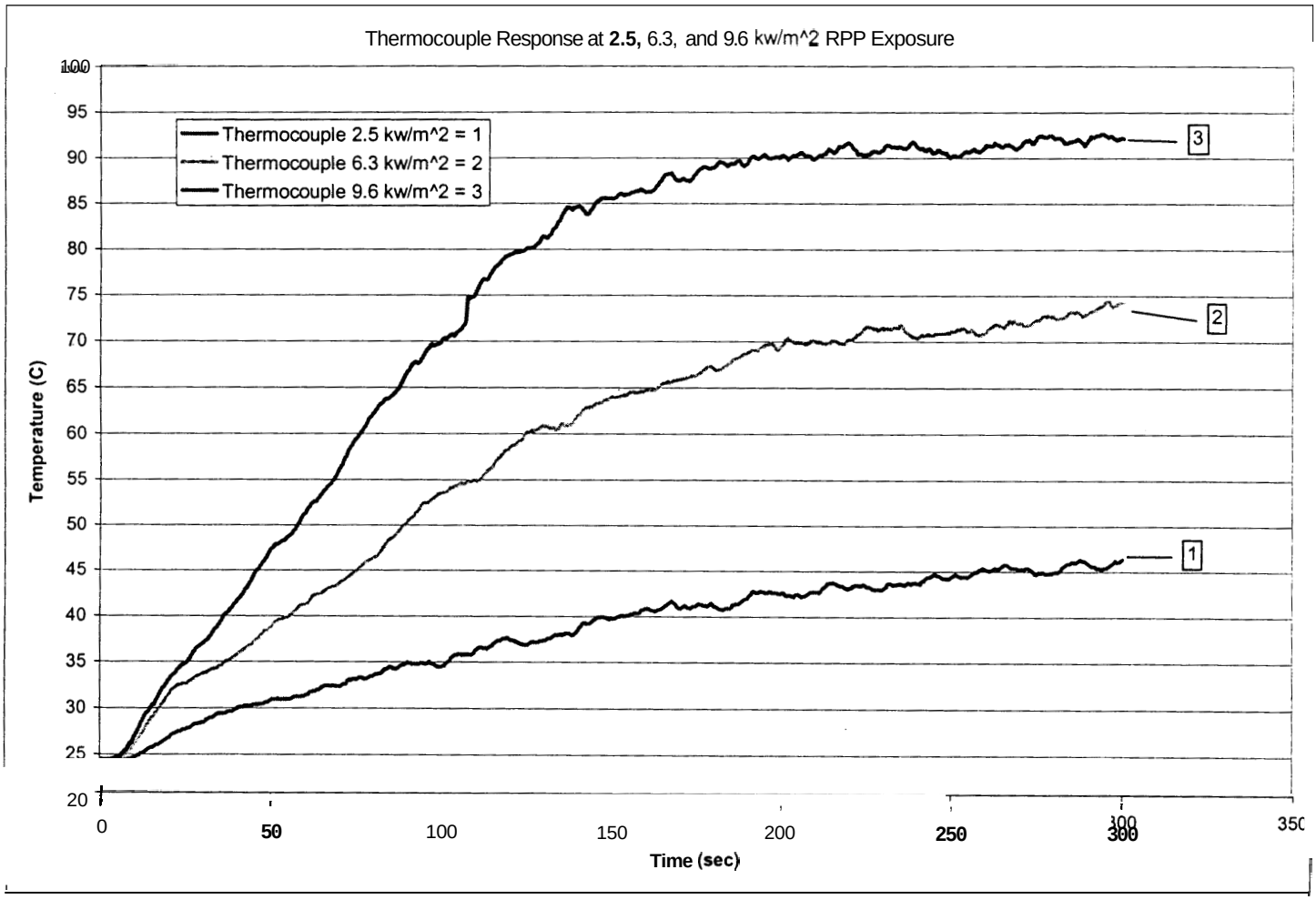

Figure 4.1 1: Thermocouple response at 2.5, 6.3, 9.6 kw/m2 RPP exposure.

Sensor	Time at 6.3 kw/m^2 (sec)	Time at 9.6 kw/m^2 (sec)
NCSU Water Cooled Prototype	130	92
Pyro-Cal	134	102
Thermogauge™	205	137
TPP	NB	230
Thermoman	NB	246
Thermocouple	112	69

Table 4.2: Time for sensors register a delta of 25% and 55%

6.3 kw/m²	**Time to register a 25°C (sec)**	**Time to register a 55°C (sec)**
Pyro-Cal	—	—
Thermoman®	214	—
TPP	211	—
Thermocouple	88	—
9.6 kw/m²	**Time to register a 25°C (sec)**	**Time to register a 55°C (sec)**
Pyro-Cal	—	—
Thermoman®	120	—
TPP	123	271
Thermocouple	57	108

Chapter 5

CONCLUSIONS

The water-cooled prototype sensor has been shown to be a useful thermal sensor for evaluating the thermal protective performance of firefighter's protective clothing in prolonged thermal exposures. Laboratory tests indicate that the NCSU Water Cooled Prototype sensor provides a consistent and stable reading over the wide range of thermal exposures of interest. It measures incident heat flux reliably and accurately over extended duration's at low exposures. In addition to the extended time of 300 seconds, the water cooled prototype sensor behaved in the same fashion for identical runs for 600 seconds providing very stable and accurate responses, which can be seen in Appendix E.

Although commercial sensors such as the Thermogauge™ and the Hy-Therm@ provided very stable and accurate responses to incident radiation, they lack the ability to detect conductive heat transfer through protective garments. These sensors are designed more for direct incident radiation exposures. This may generate misleading results in deciding how much protection a particular garment provides during a simulated firefighters exposure to heat. TPP sensor has been designed for short-term incident heat flux exposures. This creates an unusable sensor for extended measurements of incident heat flux and may also generate

misleading results in determining the amount of protection a garment may provided during exposures. In addition, the thermocouple response tends to underestimate the amount of protection a garment provides during a simulated firefighters exposure. The NCSU Water Cooled Prototype sensor has been designed for direct sensor and RPP type exposures. This new technology allows for a complete instrument for measuring incident heat flux as well as accessing the performance of firefighter turnout garments for extended duration's of exposure.

Chapter 6

FUTURE DIRECTIONS

Several issues need to be addressed with the water-cooled prototype to permit this new technology to be *fully* utilized. Experiments need to be conducted at wider range of water flow rates. Additionally, the sensor design should be to accurately mold the thermocouple into the body of the sensor. The water-cooled prototype sensor also needs to be exposed to a wider range of thermal exposures. This project only selected a range consisting of 2.5 kw/m^2 – 9.6 kw/m^2, while a range consisting of 2.5 kw/m^2 ~ 84 kw/m^2 needs to be addressed. Finally, a wider selection of turnout protective test fabrics needs to be tested. This project only tested one type of fabric while a much broader range should be viewed.

REFERENCES

1 .Abbott, N. J. and Schulman, S. *Protection From Fire: Nonflammable Fabrics and Coatings.* J. Coated Fabrics. Vol. 6. July 1976. pp. 48-62.

2. Lawson, J.R., *Fin? Fighter's Protective Clothing and Thermal Environments of Structural Fin? Fighting.* NISTIR 5804, National Institute of Standards and Technology, Gaithersburg, MD, August, 1996.

3. Weaver, J.A. and Stoll, A.M. *Mathematical Model of Skin Exposed to Thermal Radiation.* Aerospace Medicine. Vol. 40. January 1969, pp. 24 - 30.

4. Crown, E. M. and Dale, J. D. *Built for the Hot seat,* Canadian Textile Journal. March 1993, pp. 16-19.

5. Lawson, J.R. and Jason, N.H., eds. *Firefighter Thermal Exposure Workshop.* NIST Special Publication 911, National Institute of Standards and Technology, Gaithersburg, MD, 1996.

6. Foster, J. A. and Roberts, G. V. *Measurements of the Firefighter Environment-Summary Report.* Fire Engineers Journal. Vol. 55. No. 178. September 1995. pp. 30-34.

7. B. N. Hoschke. *Specifications for Firefighting Clothing.* Fire Safety Journal. April 1981, pp. 125-137.

8. James S. Johnson and S.Z. Mansdorf, Eds. American Society for Testing and Materials. West Conshohocken, PA. 1996, pp. 607 - 624.

9. Vatell Corporation, 2001 South Main Street, Blacksburg, VA 24060 (540) 961-2001.

10. Hy-Cal Sensing Products, Honeywell Inc., 9650 Telstar Avenue, El Monte, CA 91731. (800) 932-2702.

11. Grimes, R., *The Design and Calibration of a Surface Heat Flux Transducer for Use in Fabric Thermal Protection Testing,* MS Thesis. North Carolina State University. Raleigh, NC. 1993.

12. American Society for Testing and Materials. ASTM Standard F 1939-99 Standard Test Method for Radiant Protective Performance of Flame Resistant Materials

13. Stoll, A.M., and Chianta, M A. *Method and Rating Systems for Evaluations of Thermal Protection.* Aerospace Medicine, Volume 40 (1969).

14. Stoll, A.M., and Chianta, M.A. *Heat Transfer Through Fabrics as Related to Thermal Injury.* Transactions-New York Academy of Sciences, Vol. 33 (7), (1971).

15. Henriques, F.C. *Studies of Thermal Energy: V. The Predictability and the Significance of Thermally Induced Rate Process Leading to Irreversible Epidermal Injury.* Archives of Pathology, Vol. **43, p.489,** 1947.

16. Jensen, R. L., Jr., *Thermal Performance of Firefighters' Protective Clothing.* Safety and Security Systems Division, 3M Center, Building 225-4N-14, St. Paul, MN 55144-1000.

17. Neal, T.E. *Prediction of Fire Fighter* **Bum** *Injury Using* **Skin** *Model Sensors at Low Level Heat Flux Exposures- Preliminary Results.* NFPA 1971 Technical Committee. November 5,1998.

APPENDIX B

Empirical Method of Calibration

Several assumptions were made to provide a preliminary basis for estimating the rate of water flow to the prototype sensor. These assumptions are as follows:

Assumption s :

$T_1 = 21\,^{\circ}C = 294.15\,K$

$P_1 = P_{atm} = 101\,kPa$

$A_1 = 1.962 \times 10^{-5}\,m^2$

$T_2 = 31\,^{\circ}C = 304.15\,K$

$P_2 = P_{atm} = 101\,kPa$

$A_1 = 1.962 \times 10^{-5}\,m^2$

A_1 = ***Area Exposed To Heat Flux*** $= .0012\,m^2$

$q = 2\,cal / cm^2 * s$

$\rho_{H_2O} = 1000\,kg / m^3$

$C_p = 4.184\,kJ / kg * K$

Where T_1 is the temperature of the water flowing into the sensor, T_2 is the temperature of the water flowing out of the sensor, P_1 and P_2 are the pressures at the points of entrance and exit of the water. A_1 and A_2 are the areas associated with the area of the fitting for water flow in and out of the sensor. A_1 is the area

of the copper disk being exposed to the heat source. q is the associated heat flux, $_{H2O}$ is the density and C_p is he specific heat of the water at normal room temperature and pressure.

By converting q to joules and C_p to joules/gram*Kelvin, we calculated as follows:

$$q = \frac{2\,cal}{cm_{\,2} * s} * \frac{4.184\ J}{1cal} * \frac{1cm^{\,2}}{10^{-4} m^{2}} * .0012\ m^{2} = 105\ .05\ J\ /\ s$$

$$C_{p} - \frac{4.184\ kJ}{kg\ *\ K} * \frac{10^{-3}\ kg}{1\,g} * \frac{1\,J}{10^{-3}\ kJ} = 4.184\ J\ /\ g\ *\ K$$

We stipulate that, at steady state, q is equal to the mass flow rate times the specific heat times the difference in water temperature entering and exiting the sensor, T. The mass flow rate is then calculated as:

$$q = \dot{m} C_p \Delta T$$

$$105\ .05\ J\ /\ s = \dot{m}(4.184\ J\ /\ g\ *\ K)(304\ .15\ K - 294\ .015\ K)$$

$$\dot{m} = 105\ .05\ J\ /\ s \,/\, (4.184\ J\ /\ g\ *\ K)(10\ K)$$

$$\dot{m} = 2.51\ g\ /\ s$$

Proceeding to convert the mass flow rate from grams/second to liters/second.

$$\dot{m} = \frac{2.51 g}{s} * \frac{1 m^{3}}{10^{6} g} * \frac{10^{3}\ Liters}{1 m^{3}} = .00251\ Liters\ /\ s$$

Consequently, the velocity of the cooling water is determined as:

$$\dot{m} = \rho * V * A = 10^{6}\, g * V * 1.962 \times 10^{-5}\, m^{2}$$

$$V = \frac{\dot{m}}{\rho * A} = \frac{2.51\, g/s}{10^{6}\, g/m^{3} * 1.962 \times 10^{-5}\, m^{2}} = .12793 \text{ m/s}$$

Initial experiments were designed to provide a primary assessment of the sensor response to an 84.0 kw/m² (2 cal/cm²·sec) thermal exposure. An 84.0 kw/m² exposure was generated in a TPP test set up that utilized gas burners and radiant panel as the heat source. This exposure was maintained for a period of 180 seconds. The copper calorimeter sensor was cooled, throughout the exposure, by circulating water at a flow rate of 0.8 g/sec. The coolant flow rate was measured by allowing the discharged water to flow into a graduated beaker to measure the volume flow rate, which was then converted to mass flow rate.

Figure B.1 shows the manner in which the sensor temperature increased during the heat exposure. This behavior is indicative of conventional transient heat transfer response, through the first two minutes of the exposure. Beyond two minutes, fluctuations are symptomatic of air bubbles, trapped with the water within the sensor, and their effects on dynamics of the heat transfer.

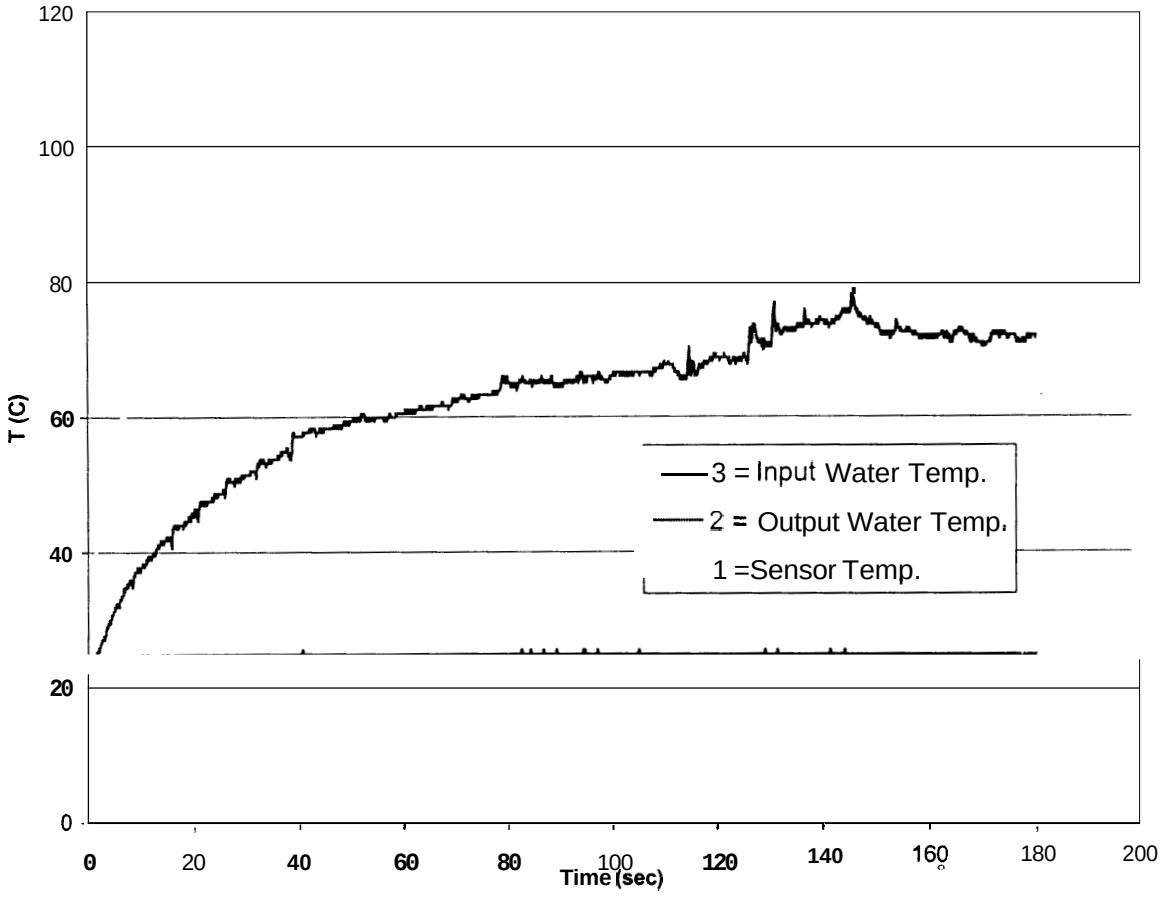

Figure B.1. Temperature response of liquid cooled copper slug calorimeter exposed to 84 kw/m^2 heat flux for 180 seconds.

After constructing the prototype and proof of concept of the liquid cooled prototype sensor preliminary laboratory testing needed to be conducted. These tests were conducted primarily to validate the basic measurement principal utilized by the sensor and to provide baseline information that will facilitate the

design and development of subsequent sensors having enhanced performance characteristics.

During this project, two different types of configurations were utilized. The TPP type configuration and the RPP type configuration. The TPP type configuration was utilized for preliminary testing and proof of concept. The TPP testing apparatus is configured horizontally. The TPP testing apparatus also contained gas burners to assist in achieving high amounts of incident heat.

The RPP type configuration has a testing apparatus configured vertically and was used for the comparative study as well as for the information contained within the main body of the thesis. Since *only* low amounts of heat were required during this project, the RPP contained no gas burners. The two different type configurations can be seen below in Figures 3 and 4 respectively.

The sensor output was fed to a state of the art data acquisition device, which consisted of four analog, thirty-two channel thermocouple amplifiers (SCXI-1102 National Instruments) mounted within a twelve slot multiplexing chassis (SCXI-1001 National Instruments). The thermocouple amplifiers, in addition to capturing nonlinear voltage readings from each sensor, isolated and linearized each signal. Output voltages were fed from the twelve slot multiplexing chassis device, to an MIO board (AT-MIO-16F-5 DAQ) to generate time signatures for

these signals. National Instruments LabView software program was used to translate voltage signals into temperature readings.

The sensor was exposed to the following conditions to evaluate characteristics and response:

- Condition1

100% radiant heat source @ 6.3 kW/m^2 bare exposure for 300 seconds

Heat Source: Bank of nine quartz tubes.

- Condition2

100% radiant heat source @ 9.6 kW/m^2 bare exposure for 300 seconds

Heat Source: Bank of nine quartz tubes.

- Condition 3

50/50 convective/radiant heat source @ 52.5 kW/m^2 bare exposure for 300 seconds

Heat Source: TPP test configuration flames and bank of nine quartz tubes.

- Condition4

50/50 convective/radiant heat source @ 84.0 kW/m^2 bare exposure for 300 seconds

Heat Source: TPP test configuration flames and bank of nine quartz tubes.

Coolant Flow Rate Dependency

Heat transfer calculations, based on thermal energy balance in the sensor system, have indicated that the source of system instability is the relatively low water flow rate chosen for the initial experiment and can be seen in appe. These calculations indicated that, to evaluate the thermal energy absorbed by a 12 cm^2 copper disc exposed to 2.0 cal/cm^2·sec with a water coolant (c_p = 4.184 J/g°k), while maintaining a 10°C temperature differential between the copper sensor and water coolant will require a flow rate of approximately 2.5 g/sec (significantly higher than the 0.8 g/sec flow rate used for the first experiment.

Experiments continued to evaluate the response of the new sensor using higher water flow rates to minimize measurement instabilities related to the formation of air bubbles with the water coolant.

The emphasis of the experiments were conducted to qualifying the response of the sensor when exposed to different levels of thermal energy. Defining the relationship between the flow rate of the water coolant and sensor exposure to incident heat was equally as important. The sensor has been exposed to incident

thermal energy ranging from 6.3 to 84 kw/m^2 (0.15 to 2.0 $cal/cm^2 \cdot sec$) for a period of 5 minutes. Throughout these exposures, the copper calorimeter sensor was cooled with water flowing at rates from 0.94 to 2.33 g/sec. Figure B.2 provides a typical example of the data generated in these experiments, the sensor was exposed to 6.3 kW/m^2 (0.15 $cal/cm^2 \cdot sec$) radiant heat with a water flow rate of 0.94 g/sec. The output shows the measured sensor temperature, and the entrance and exit temperatures of the circulating water. Figure B.3 shows the difference between the rise in temperature of the sensor and the rise in coolant temperature (At) plotted as a function of exposure time. Figure B.4 shows the experimentally determined relationship between At and incident heat flux.

These experiments provided insights for utilization of the prototype sensor. They indicate that the sensor response stabilizes within 15 seconds of a 300-second exposure to heat. They show that the sensor response is linearly related to the heat flux level of the exposure (Figure B.4). This is a significant finding since it verifies that the heat flux can be calibrated and reliably predicted from the instrument output. Experiments have also revealed that a coolant flow rate within the ranges of a minimum rate 0.94 g/sec and 2.33g/sec sensor temperature rise is non-dependent of the flow rate of the water (Figure B.5).

Initially, it was thought that by calibrating the sensor output to the incident heat flux and using the delta t (t) of the sensor output, the unknown incident heat

flux on the sensor could be accurately predicted. Indeed this is true, but a better understanding of the operation of the prototype sensor needed to be established in order for the prototype to be operated assuredly in a wider environment. With this in mind, the prototype sensor was slightly modified by adding an additional thermocouple to the sensor housing. The sensor housing, being constructed of brass rather than copper, needed to have the amount of energy being transferred into the water established as it passes through the prototype sensor. After the amount of energy being transferred through the copper disk and amount of energy being transferred from the sensor housing into the water was understood, a complete mathematical model could be constructed to fully establish the operation of the cooled prototype sensor.

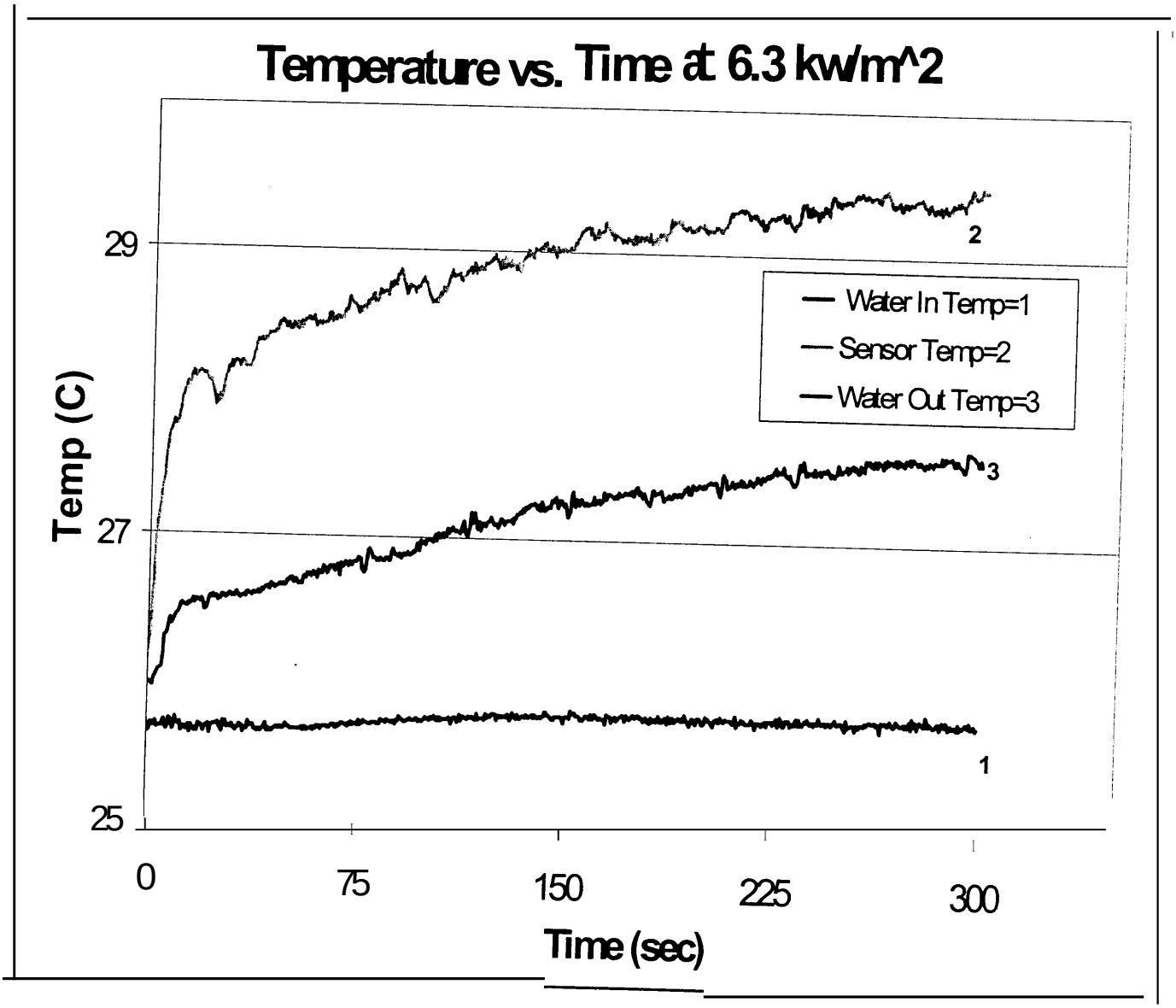

Figure B.2: A plot of sensor temperature, entrance and exit coolant temperature vs. time for a 6.3 kw/m2 for a 5 minute exposure.

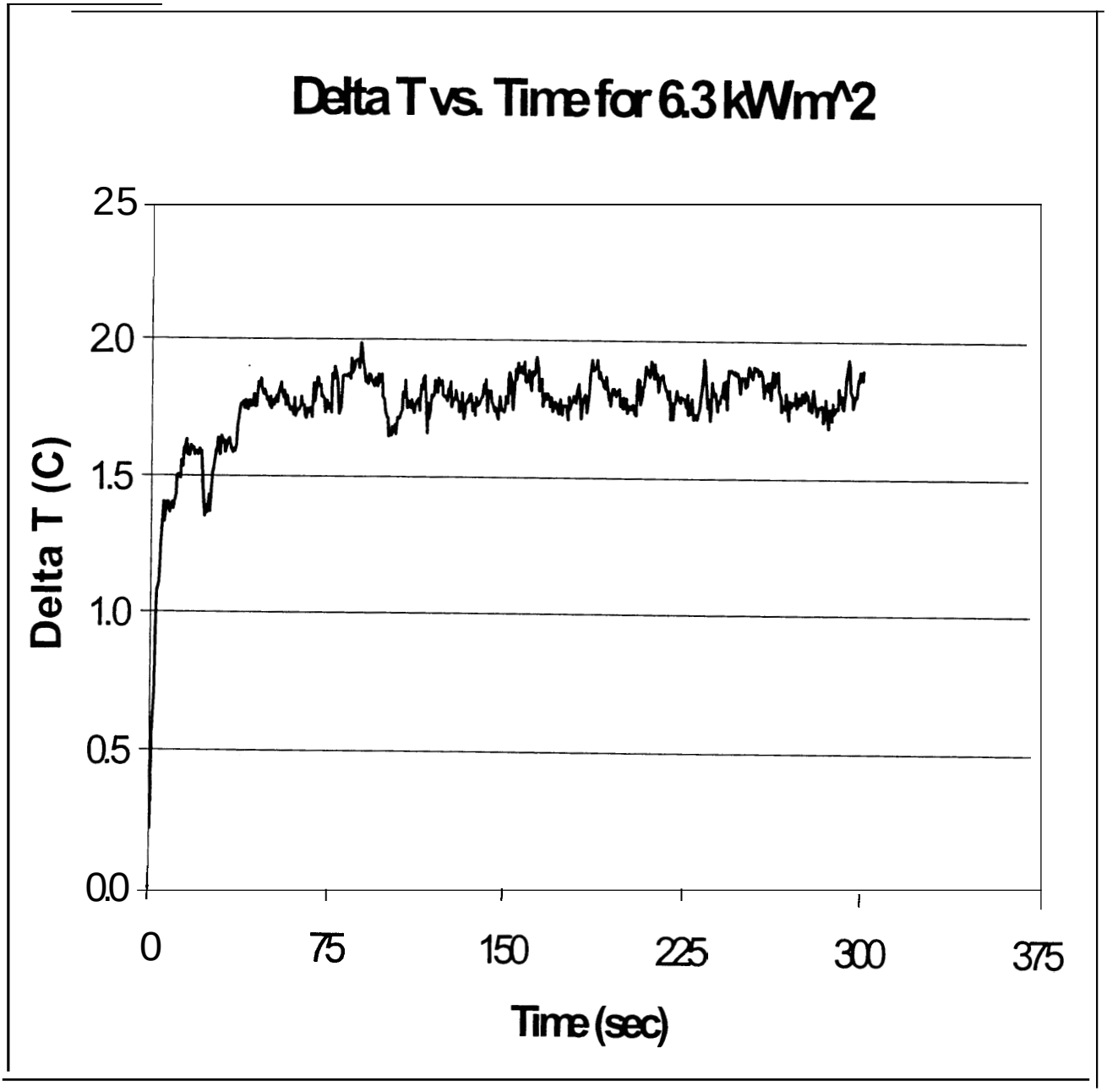

Figure B.3: A plot of the difference between the rise in temperature of the sensor and the rise in coolant temperature (At) as a function of exposure time for an exposure of 6.3 kw/m^2.

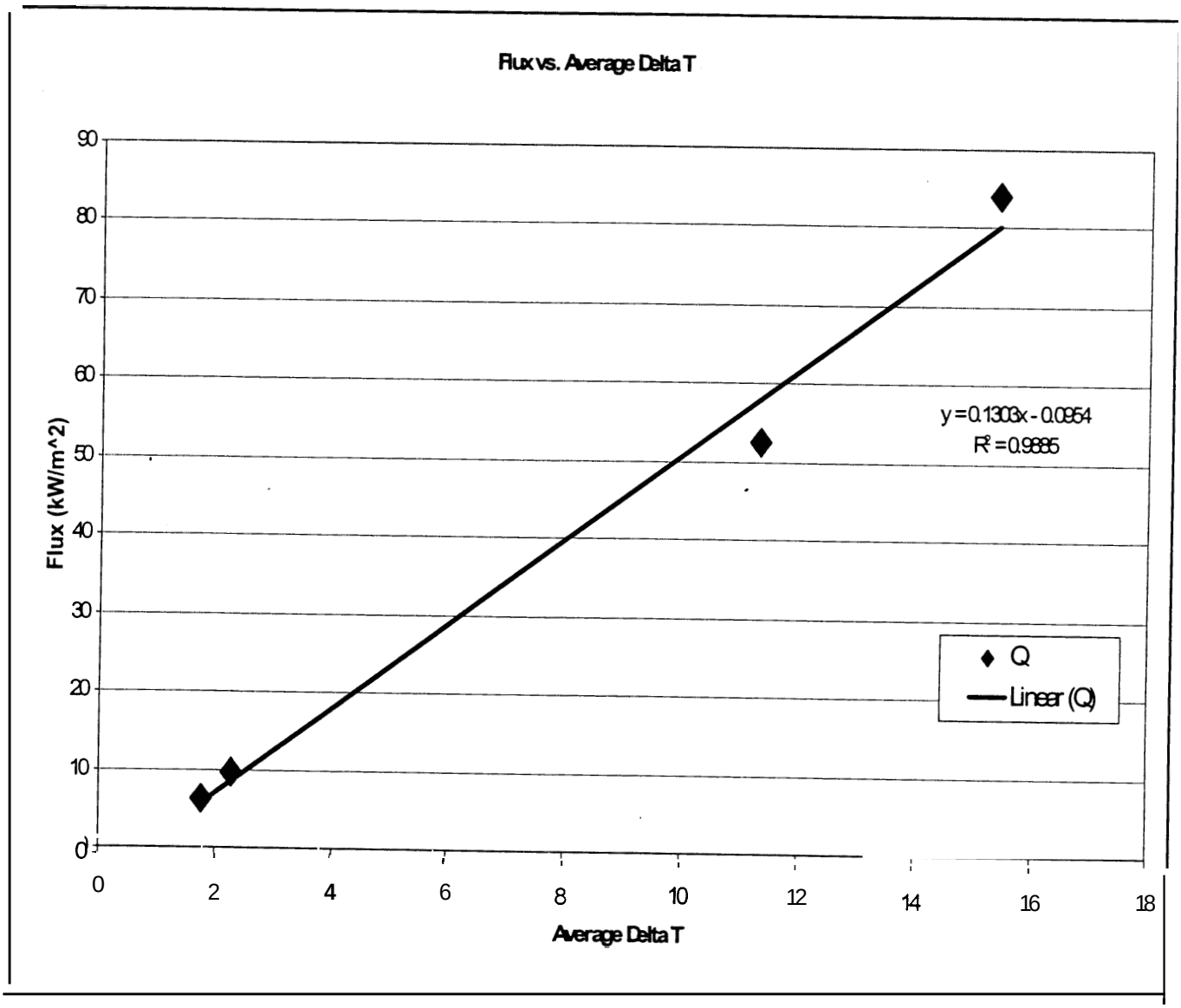

Figure **B.4:** A plot of the average temperature difference between sensor temperature and the exiting temperature of the coolant **vs.** incident heat flux for 6.3 kw/m^2.

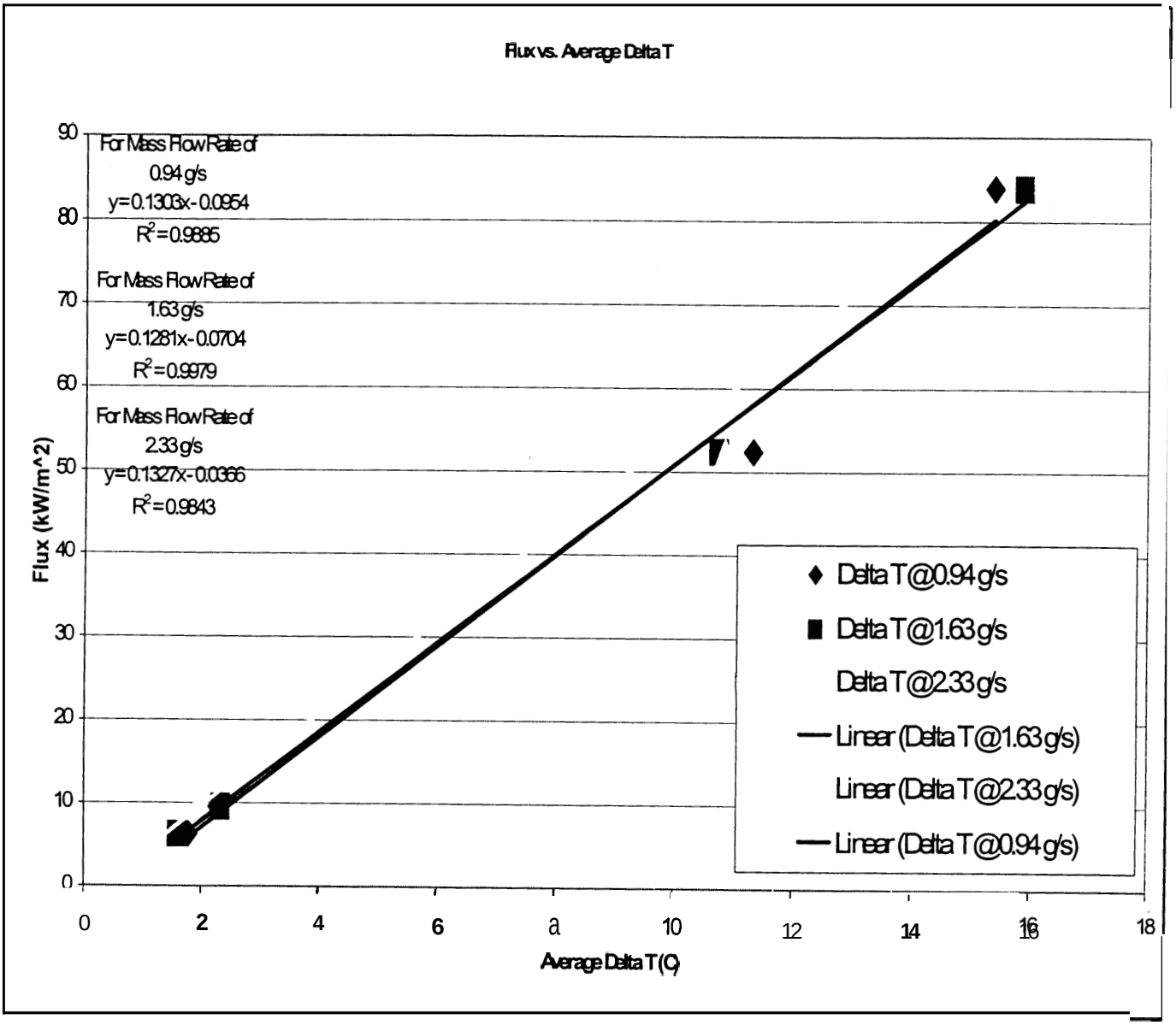

Figure B.5: A plot of the average difference in temperature between copper slug sensor and the temperature of the exiting coolant vs. incident heat flux for exposures ranging from 6.3 to 84 kw/m^2.

APPENDIX *C*

Fabric Mounting and Testing Details

A data acquisition system took information for 300 seconds and that information was stored in a spreadsheet file for later use. The sensor to be tested was tested triplicate measurements allowing time between each trial for sensor cooling.

For the RPP type configuration, in order for the sensor face to be in intimate contact with the fabric, the following procedure was followed:

- Fire fighter composite turn out was placed on a hard surface with a 6 inch by 6 inch square, 160 gram weight placed atop the fabric assembly and measured for the height, excluding the height of the weight (figure C.1).

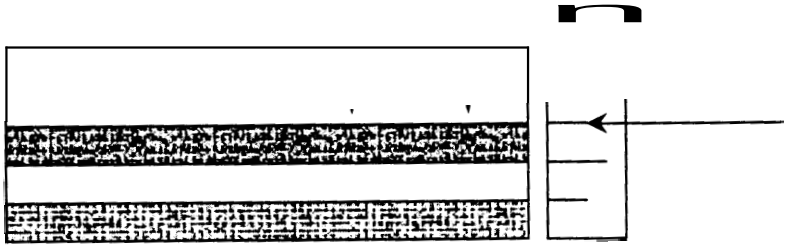

Figure C.1: Display of thickness measurement.

- Fire fighter composite turnout was then compressed to the fullest and re-measured for the height (figure C.2).

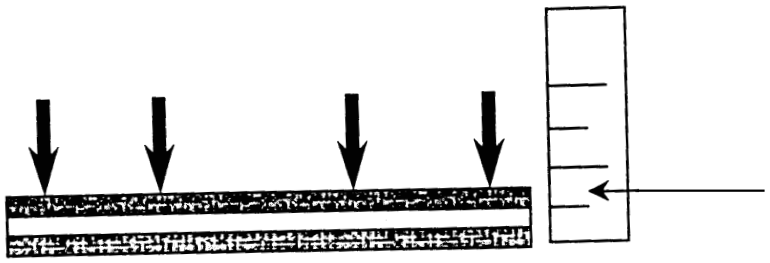

Figure C.2: Display of compressed thickness measurement.

- The two measurements were then subtracted and the result was the thickness in which a spacer was placed between the fabric and the fully compressed, supporting restraint in the holder in order to provide consistency in mounting conditions as well as to provide intimate contact with the sensor face and the test garment.

The NCSU Water Cooled Prototype sensor was mounted in the insulation block and the coolant was pumped through the system. The discharged coolant was collected into a graduated beaker to measure the volume flow rate of the coolant through the system. After the coolant flow rate had been established the sensor was exposed for 300 seconds. Measurements of the copper disk, sensor housing,

incoming, and discharge coolant temperatures of the prototype sensor were gathered by the data acquisition system.

The remaining liquid cooled sensors were also mounted in the same fashion in the center of an insulation block including the spacers; coolant was then pumped through the system and exposed to the calibrated heat source for 300 seconds. The output signals from the sensors were gathered by the same data acquisition system. The non-cooled sensors were arranged in the same manner as described above excluding the coolant circulation and exposed to the calibrated heat source for 300 seconds. Triplicate measurements were conducted at each exposure condition of 2.5, 6.3, and 9.6 kW/m^2 and for each sensor.

APPENDED

Heat Flux Calculation of Sensors.

#1 Thermogauge™

The signal output from the Thermogauge™ sensor was recorded as a milli-volt / time. The milli-volt signal was then multiplied by a factor of 0.93 BTU/ft²*sec/mV provided by the manufacturer in order to convert the milli-volt output from the sensor directly to heat flux in BTU's/ ft²*sec.

#2 Hy-Therm@

The signal output from the Hy-Therm@was recorded as a milli-volt / time output. The signal was then divided by a factor of 16.83 BTU/ft²*sec/mV provided by the manufacturer in order to convert the milli-volt output from the sensor directly to heat flux in BTU/ft²*sec.

#3 Pyrocal

The signal output from the Pyrocal sensor was read in as a time / temperature measurement in degrees Celsius. From this, the following equation was used to compute heat flux:

$$q = \frac{MC_P C_1}{A} * \frac{dT}{dt} + K_l (T_d - T_i)$$

Where:

q : Incident heat flux (cal/cm^2·sec)

M : Mass of calorimeter slug (grams)

C_P : Heat capacity of copper (cal/g °C)

C_1 : Thickness factor as experimentally determined

A : Disk area (cm^2)

K_l : Heat loss coefficient as experimentally determined (cal/cm^2·sec· °C)

T_d : Surface temperature of disk at time t (°C)

T_i : Initial or ambient temperature (°C)

#4 Thennoman (or skin simulate)

The signal output from the Thermoman sensor was recorded as a time / temperature measurement. A computer program based on a reverse heat flux calculation was used to estimate the heat flux.

#5 TPP

The TPP sensor signal output was captured as a time/ temperature signal. The following equation was then used to calculate heat flux.

$$\frac{MC}{A \quad dt}$$

Where,

M :Mass of calorimeter slug (grams)

C_p Heat capacity of copper (cal/g °C)

A :Disk area (cm^2)

APPENDIX E

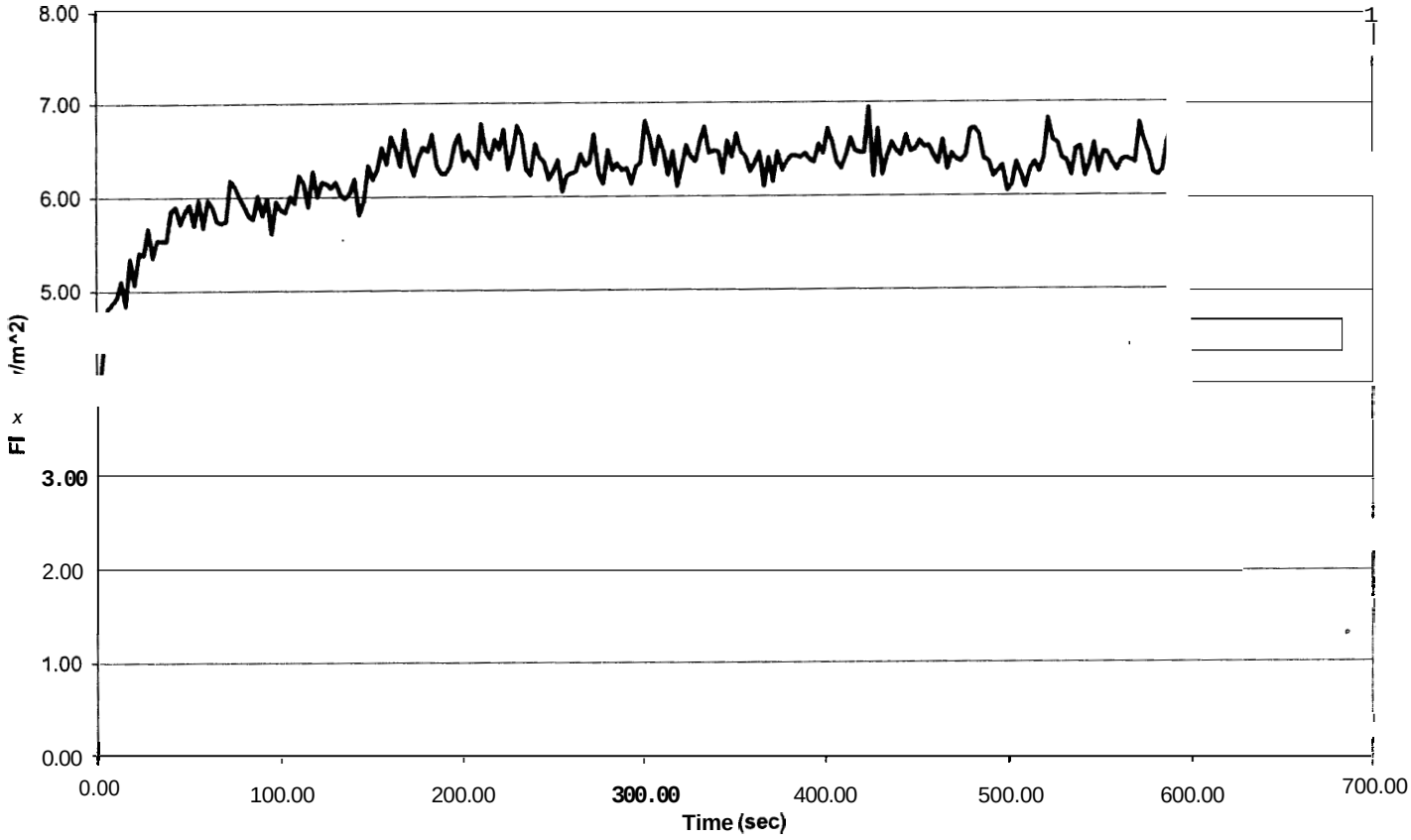

Figure E. 1: Response of NCSU Water Cooled Prototype at 6.3 kilowatts/m^2 for 600 seconds